Inference and quantification of peptidoforms in large sample cohorts by SWATH-MS: Supplementary Notes

George Rosenberger,[1,2,*] Yansheng Liu,[1,*] Hannes L Röst,[1,3] Christina Ludwig,[1,4] Alfonso Buil,[5] Ariel Bensimon,[1] Martin Soste,[6] Tim D Spector,[7] Emmanouil T Dermitzakis,[8] Ben C Collins,[1] Lars Malmström,[1,9] and Ruedi Aebersold[1,10,†]

[1]*Department of Biology, Institute of Molecular Systems Biology, ETH Zurich, Zurich, Switzerland*

[2]*PhD Program in Systems Biology, University of Zurich and ETH Zurich, Zurich, Switzerland*

[3]*Department of Genetics, Stanford University, Stanford, CA, USA*

[4]*Bavarian Biomolecular Mass Spectrometry Center (BayBioMS), Technical University Munich, Freising, Germany*

[5]*Research Institute of Biological Psychiatry, Mental Health Center Sct. Hans, Boserupvej 2, Roskilde, Denmark*

[6]*Department of Biology, Institute of Biochemistry, ETH Zurich, Zurich, Switzerland*

[7]*Department of Twin Research and Genetic Epidemiology, King's College London, St Thomas' Hospital Campus, London, UK*

[8]*Department of Genetic Medicine and Development, University of Geneva Medical School, Geneva, Switzerland*

[9]*S3IT, University of Zurich, Zurich, Switzerland*

[10]*Faculty of Science, University of Zurich, Zurich, Switzerland*

(Dated: May 20, 2017)

*These authors contribute equally to this study

†Corresponding author: aebersold@imsb.biol.ethz.ch

Contents

I. INFERENCE OF PEPTIDOFORMS

IPF is implemented in C++ and Python in the OpenSWATH[1] TOPP[2] applications as part of OpenMS[3] and PyProphet[4] and distributed under the Modified BSD License. It consists of three main components that support sequential steps of the methods (see Figure S1):

A. Step 1: Query parameter generation

The purpose of this step is the generation of spectral libraries representing different peptidoforms that are subsequently used to query SWATH-MS or DIA data sets. The input for this step are spectral libraries or transition lists assigned to peptidoforms at low to high confidence. A low confidence spectrum library can for example be generated by open modification searching of DDA or DIA data. Alternatively, low confidence transition lists could be derived from the unmodified peptidoform or entirely *in silico* based on a hypothesis. Spectral libraries of medium or high confidence sequence assignments could originate from database search with selected modification types and optional site-localization post-processing[5]. The ideal strategy should be selected based on the research question and availability of suitable data sets, e.g. acquired by DDA mass spectrometry of PTM enriched samples, with tradeoffs regarding the comprehensiveness and sample representation. Based on the input, the algorithm generates spectral libraries in TraML[6] format consisting of two different transition types, *detection transitions* and *identification transitions*.

Detection transitions are used to detect candidate peptide signals (peak groups) at the MS2-level as described before for targeted analysis of DIA data sets[1,7]. They consist of precursor and product ion m/z values from spectral libraries, the reference relative library intensities and reference normalized retention time for target chromatogram extraction, peak group detection and scoring using OpenSWATH[1]. These transitions are commonly only peptide sequence-specific[8], but with specific transitions, they can favor the detection of matching peptidoforms[9,10]. For this reason, multiple peptidoforms in the input spectral libraries will be represented by multiple independent sets of peptide query parameters.

Identification transitions are generated *in silico* by the algorithm. Taking into account

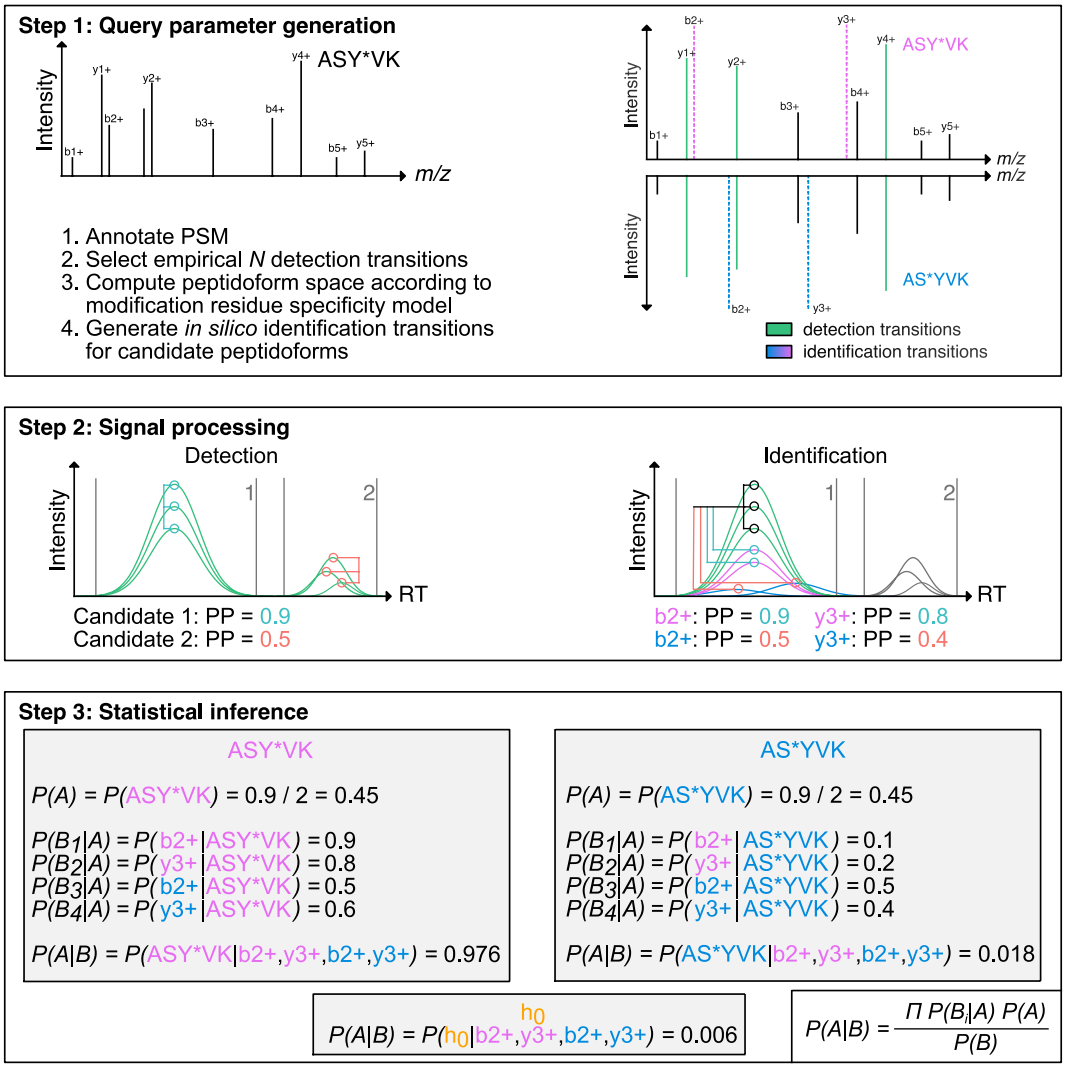

Figure S1: **IPF analysis workflow overview. a)** Query parameter generation: Based on a discovery proteomics workflow (DDA or DIA), peptide query parameters consisting of *detection* and *identification transitions* for all peptidoforms are generated. **b)** Signal processing: Using a two-tier scoring approach, the *detection* and *identification transitions* are extracted from the SWATH maps. The *detection transitions* are used to find candidate peak groups against which the identification transitions are scored. The two-tier scoring estimates posterior probabilities (PPs) for the candidate peak groups using the *detection transitions*. In the step on transition-level, the PPs that individual *identification transitions* are originating from the peak group associated peptide are estimated.

Figure S1: **c)** Statistical inference: A Bayesian hierarchical model (BHM) integrates the transition PPs according to residue specificity to peptidoform PPs. In addition to the peptidoforms, the PP that the signal is a false positive (h_0) is being updated. In data sets with large precursor isolation windows, the BHM is extended by an intermediate layer to adjust the probabilities using precursor data on MS1 and MS2-level data (see Methods).

either the precursor *m/z* error tolerance on the MS1-level or the swath acquisition setup on the MS2-level and modification type residue specificity (default: UniMod & PSI-MOD), the peptide query parameter generation step will consider in an unbiased manner all potential peptidoforms and site-localizations for each set of peptide query parameters that fall within the same precursor isolation window. Importantly, for these peptidoforms, all theoretical fragment ion spectra are generated and the resulting product ions are annotated with their associated peptidoforms. In an analogous manner the algorithm generates decoy *identification transitions*, which are not used as null distribution for peak group detection, but for the assessment of individual *identification transition* confidence in the second step of peptidoform inference (see below). Additionally, the unfragmented precursor ion *m/z* values can be used and added as *identification transitions* to support precursor detection in setups with large precursor isolation windows.

The output of this step is a hybrid spectral library, consisting of the different transition types, annotated with their specific scoring attributes (detection and/or identification, target or decoy) that can be automatically extracted, scored and integrated to peptidoforms by the downstream algorithms.

B. Step 2: Signal processing

The purpose of this step is to query and score the targeted peptides from the raw SWATH-MS data. In DIA mode, the most important parameters to adjust for peptidoform specificity and sensitivity is the precursor isolation window width and the optional MS1 acquisition or dwell times. A signal detection and extraction algorithm (Figure S2) is applied to the input DIA data to score the ion chromatograms on the MS1- and MS2-levels.

Prior to peak picking and scoring, all ion chromatograms according to the spectral library are extracted. To boost detectability of the candidate peak groups, for peak picking and the first scoring tier, only the (previously empirically-observed) *detection transitions* are considered. This step is as previously described[1]. In the second scoring tier, scores[1,7] are computed for each individual *identification transition* characterizing co-elution and shape-similarity against the detection transitions. Additional scoring values generated include signal-to-noise, mass deviation, isotope overlap and isotope correlation between observed and expected fragment ion *m/z* (see Methods). In addition, precursor ion chromatograms are extracted from the MS1 and MS2 maps according to the peptide query parameters[11]. The precursor chromatograms are scored against the *detection transitions* using the mProphet and OpenSWATH peak shape, coelution and mass accuracy scores[1,7].

The output of this step are the scores for candidate peak groups and their *identification transition* and precursor chromatograms.

C. Step 3: Statistical inference and error-rate control

The purpose of this step is to infer the set of correctly identified peptidoforms at a particular q-value or FDR. This is accomplished by processing the scored MS1-, MS2- and transition-level candidate peptide signals by a multi-level, semi-supervised learning algorithm, followed by peptidoform inference employing a Bayesian hierarchical model (Figure S1).

Semi-supervised learning: On the MS1, MS2 and transition level, respectively, the set of scores is combined to a single discriminant score by a semi-supervised learning algorithm that uses decoy peak groups or transitions as negative and the best scoring target peak groups or transitions as positive set[1,7,12]. The distributions on MS1, MS2 or transition-level scores have properties reflecting their different signal quality and strength (Figure S2): On the MS1-level, the ratio of false targets versus true targets is commonly higher than on MS2-level, since the signal is less discriminative. On the transition-level, usually a larger fraction of false target transitions is included that are caused by the extraction

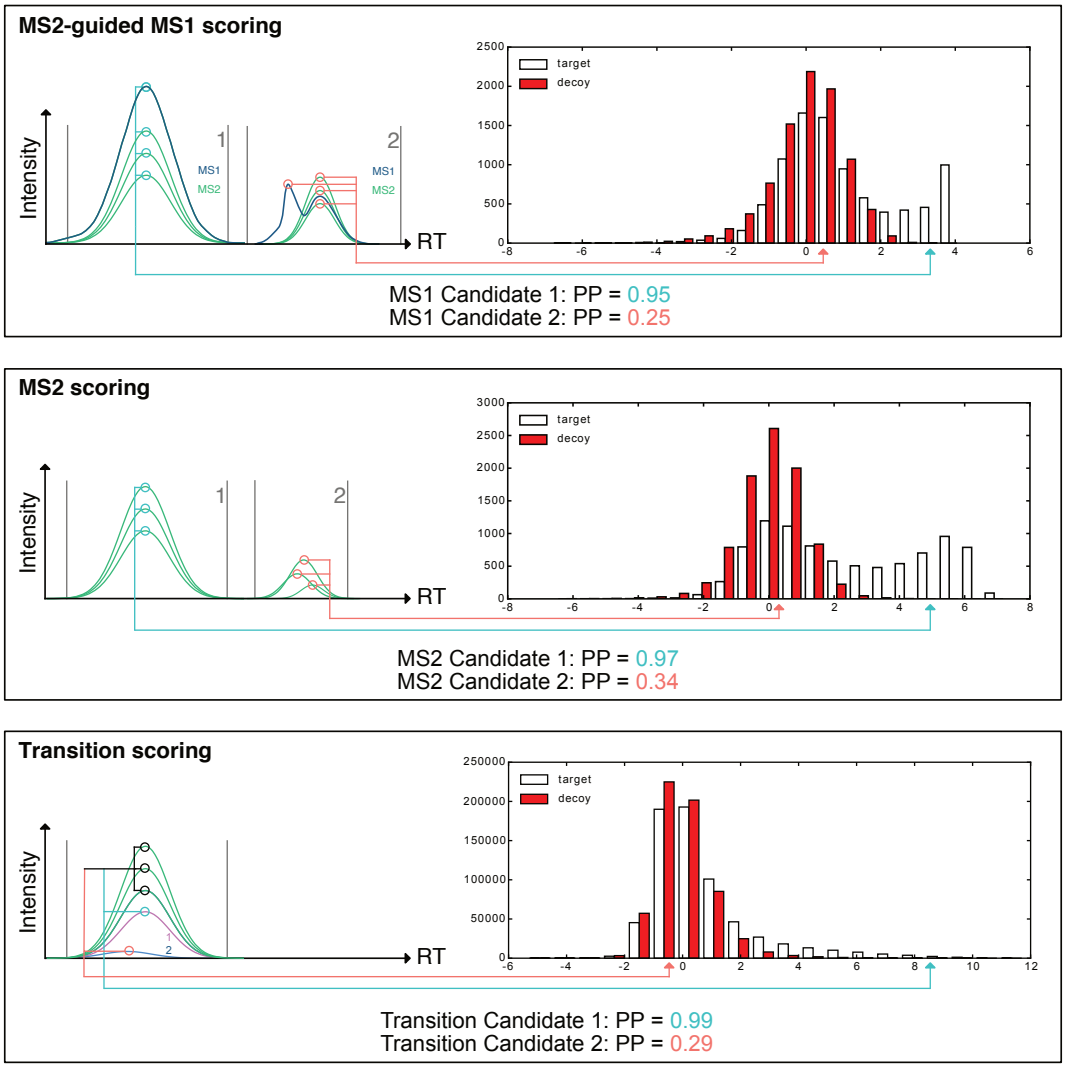

Figure S2: **Discriminant score histograms on MS1-, MS2- and transition-levels used for multi-tier scoring on the synthetic phosphopeptide reference data set.** Instead of assuming a normal distribution for false targets and decoys, a non-parametric model is used on all levels. **a)** On MS1-level, only a small fraction of the targets can be detected with confidence. **b)** MS2-level feature detection enables more sensitive peak group detection than the MS2-guided MS1 scoring. **c)** Only a small fraction of the target transitions can be detected by the transition scoring after MS2 scoring (peptide query FDR 1%) because the number of theoretical transitions exceeds by far the number of detectable fragment ions.

of *in silico* transitions which have a lower likelihood of being detectable than previously empirically observed *detection transitions*. On all levels, independent q-values and posterior error probabilities for the candidate peak group and transition signals are estimated, using non-parametrical methods[13,14].

Bayesian hierarchical modeling: In this step, the posterior probabilities (PP) are used by a Bayesian hierarchical model (BHM) to propagate the confidence of detection from peak group- and transition- to the precursor and peptidoform-levels. A first Bayesian model is applied to integrate the confidence from the (peptide sequence-specific) peak group-level and the precursor signals on MS1 and MS2-levels. This updates the peak group-level posterior probability to the precursor-level. Second, the priors for each peptidoform based on the user-specified model for modification residue specificity (e.g. STY residue specificity for phosphorylation and -98 neutral losses) and the precursor-level PP are used and updated using the detection confidence from the *identification transitions*. Especially for complex peptidoforms (e.g. when carrying multiple modifications or modifiable residues), not many unique ion signature (UIS)[15] (also referred to as diagnostic or site-determining) transitions are detectable. The BHM also makes use of the shared transitions and will attribute them to the corresponding peptidoforms, enabling partial site-localizations in ambiguous cases.

The resulting local false discovery rate (local fdr) is identical to the posterior error probability and enables direct interpretation of the confidence for each peptidoform[16]. For large-scale experiments, the error rate is commonly controlled using q-values or the global false discovery rate (global FDR). IPF provides both metrics, which can also be used for transfer of identification confidence using downstream tools for targeted proteomics like the between-measurement alignment tool TRIC[17].

II. ALGORITHMIC METHODS

A. Query parameter generation

The main workflow of peptide query parameter generation closely resembles previous approaches[1,18]: First, a standard shotgun database search[19,20], error-rate control[21,22] and spectral library generation including consensus summarization of peptide spectra[23] and RT normalization[24] is conducted. Based on these results, `OpenSwathAssayGenerator` selects transitions according to a set of rules[18]:

Rules for selection of *detection transitions*:

1. Select empirically observed fragment ion classes and allowed charge states (default: y, b; 1+ to 4+), with or without neutral losses (default: without).

2. Filter to include only transitions where product m/z does not overlap with the target SWATH-MS acquisition scheme precursor isolation window.

3. Select N most intense fragment ions (default: $N = 6$).

4. Require at least M valid fragment ions to include peptide query parameters in library (default: $M = 6$).

Peptide query parameters consisting of transitions for detection of peak group candidates generated according to the algorithm have been shown to be peptide sequence specific even in complex proteomes[8] and portable between different instrument types[25] and LC setups[24]. Using only a selection of empirically observed intense transitions has the benefit to increase the signal-to-noise characteristics of the mProphet and OpenSWATH scores[1,7], but does not enable specificity on peptidoform-level.

For this reason, the IPF tool `OpenSwathAssayGenerator` enables generation of additional *identification transitions* that are appended to the standard transitions but are treated differently than the *detection transitions* by the signal processing module (see below). *Identification transitions* are generated completely *in silico* according to the following algorithm:

Rules for generation of *identification transitions*:

1. Generate target transition map: For all sets of peptide query parameters of the same stripped ("naked") peptide sequence that fall into the same precursor isolation window (MS1 or swath window), compute all theoretical fragment ions (including the unfragmented precursor ion) according to selected ion classes and allowed charge states (Figure S1a). Further, according to the specified model of modification residue specificity (OpenMS; default: Unimod & PSI-MOD), all theoretical combinations of PTMs are computed using for each modification type the binomial coefficient indexed by n modifiable residues (including C/N-terminal modifications) and K modifications. If different modification types are present, all permutations are generated as well and the transitions are appended to the target transition map.

2. Generate target *identification transitions*: From the set of all theoretical peptidoforms falling into the same precursor isolation window, a unique set of transitions is generated. Using a specified product *m/z* threshold (default: 0.025 Da), overlapping or interfering transitions are identified and annotated. The unique set of transitions (commonly $N = 50-100$), mapping to $1-X$ peptidoforms, is appended to the spectral library consisting of *detection transitions*.

Rules for generation of *decoy identification transitions*:

1. Generate decoy sequences: A modified target-decoy approach[26] based on the previous algorithm[1] is applied. Instead of shuffling the peptide sequence, a random sequence of the 20 amino acids is used as template with identical length as the target. All modifiable residues including those carrying the modifications are used to substitute the decoy sequence at the exact location of the target sequence. This results in peptide sequences that have the exact properties in terms of modifications but a different sequence.

2. Generate decoy transition map: Similar as described above, a theoretical decoy transition map is being generated. The main difference is that the peptidoform permutation is inferred from the target sequence to derive the exact same PTM properties for de-

coys as for targets. While the product m/z is computed from the decoy sequence, the precursor m/z and normalized retention time is used from the target sequence.

3. Generate decoy *identification transitions*: Identically as above, decoy *identification transitions* are being generated. A final additional step ensures that decoy *identification transitions* are not overlapping or interfering with the corresponding target *identification transitions* by removing the decoy transitions. For phosphorylation on S, T or Y, this usually removes 5-10% of the decoy transitions.

B. MS2-guided MS1 scoring

Extraction of precursor ion chromatograms from DIA-MS1 maps (MS1 Filtering) has been shown to enable accurate precursor quantification on both DDA-MS2[27] and DIA-MS2 / SWATH-MS[11] acquisition methods. Recently, the mProphet[7] scoring system has been extended to the precursor isotope envelope[28]. For IPF, we extended this scoring approach to compute the chromatographic coelution and shape scores of the precursor ion against the fragment ion chromatograms. This results in a set of MS2-guided MS1 scores that can either be used in addition to the standard OpenSWATH scores to support the MS2-level peptide query error-rate estimation or to compute a dependent MS1-level confidence: By only using the MS2-guided MS1 scores of both targets and decoys, a separate PyProphet analysis iteration was conducted. Using the same assumptions as on MS2-level, the peptide query FDR represents the q-value that the MS1 signals and the transitions extracted from the SWATH-MS maps originate from the same peptide.

We found that MS2-guided MS1 scoring enables particularly in DIA acquisition schemes with wide precursor isolation window schemes[8] assessment of the confidence that a peak group detected a specific precursor. The reported q-value can be used independently or together with the MS2-level q-value. Especially when considering closely related peptidoforms[29], this functionality increases specificity and enables additional filtering criteria.

C. Transition scoring

The transition scoring in IPF is implemented similarly as the MS2-guided MS1 scoring: *Detection transitions* are extracted from the SWATH-MS maps and candidate peak groups and their chromatographic boundaries are being detected as described previously[1]. In addition, the *identification transitions* (and optionally, the unfragmented precursor ions) for one or multiple closely-related peptidoforms are extracted. These fragment (and precursor) ion chromatograms are scored individually against the *detection transitions*, resulting in a set of dependent coelution and shape scores as the MS2-guided MS1 scoring. In addition, spectrum dependent scores of OpenSWATH are computed and reported on transition-level.

In a multi-tier scoring approach, detected candidate peptide signals on MS1- or MS2-level above a confidence threshold are selected and the set of transition target and decoy scores is used to conduct a global (across all candidate peak groups), separate semi-supervised learning step. The resulting discriminate score and the q-value are reported on transition-level, representative of the confidence that an *identification transition* originates from the same peptidoform as the candidate peptide signals on MS1- or MS2-level.

D. Posterior error probability estimation

Conversion of discriminant scores or q-values to posterior error probabilities (PEPs) is non-trivial[16,21]. Here we employ the non-parametric target-decoy approach[13] implemented in QVALITY[14]. The QVALITY executable is directly accessed and wrapped from within PyProphet to compute PEPs using the discriminant score. The density plots of decoy and false-target transitions indicates that a non-parametric approach is suited for this data type (Figure S2).

E. Confidence propagation to peptidoform-level

Confidence propagation from peptide-spectrum match (PSM) to protein groups per data set was originally developed within ProteinProphet[30] and has been extended in several related concepts and methods[31]. The majority of the methods employ Bayesian statistics to integrate different evidence from individual peptides to proteins. For IPF, a Bayesian

hierarchical model is employed to integrate the different types of evidence from peak group-, precursor- and transition- to peptidoform-level. First, because SWATH-MS data is commonly acquired with wide precursor isolation windows, precursor-level inference is conducted. Second, *identification transitions* provide support or oppose a set of peptidoforms and are associated with a certain confidence.

The following generic assumptions are made:

1. Candidate MS2-level peak groups are independent from each other. While it can be expected that a peptidoform (co-)elutes in a standard bottom-up proteomics LC setup as a single chromatographic peak, misidentification, inconsistent peak boundaries, local saturation of the peak capacity or similar chromatographic effects can result in multiple peak groups originating from the same peptidoform. The proposed statistical model treats all candidate peak groups independently and for downstream analysis only the best scoring candidate peak group is used for further considerations.

The following assumptions are made for precursor-level inference:

1. Precursor signals on MS1 and MS2-level (considering unfragmented precursors due to insufficient fragmentation) are conditionally independent from each other and were thus considered as independent evidence for a particular peptide sequence and precursor mass.

2. The priors for correct detection (h) or incorrect detection (h_0) of the precursor are derived from the MS2-level candidate peak group (pg) posterior error probability (PEP_{pg}) as described above:

$$P(h) = 1 - PEP_{pg},\ P(h_0) = PEP_{pg}$$

3. The conditional probability for each precursor signal B_i $P(B_i|A)$ is defined as $1-PEP_i$ if hypothesis A is $A = h$ and PEP_i if $A = h_0$. PEP_i is defined as the posterior error probability of the precursor-level signal B_i as described above.

4. The marginal probability is defined as:

$$P(B) = \sum_{A}(\prod_{i}(P(B_i|A)) * P(A))$$

5. The posterior probability of hypothesis h for a candidate precursor can thus be defined as:

$$P(h|B) = \frac{(\prod_i P(B_i|h)) * P(h)}{P(B)} = \frac{P(B_{MS1}|h) * P(B_{MS2}|h) * P(h)}{P(B_{MS1}|h) * P(B_{MS2}|h) * P(h) + P(B_{MS1}|h_0) * P(B_{MS2}|h_0) * P(h_0)}$$

The following assumptions are made for peptidoform-level inference:

1. Transitions are conditionally independent from each other and provide independent evidence for a particular peptidoform; identically to the assumption that PSMs provide independent evidence for a protein group[30,32].

2. The null hypothesis (the signal is not significant or not originating from the peptide sequence) of the candidate peak group on MS1- and MS2-level is propagated and annotated as h_0 from the above precursor-level posterior probability with:

$$P(h_0) = 1 - P(h|B)$$

3. The priors for each candidate peptidoform F are defined as:

$$P(F) = \frac{1 - P(h_0)}{N_{Peptidoforms}}$$

with $N_{Peptidoforms}$ representing the total number of potential peptidoforms (without h_0). A defines the set of hypotheses including all peptidoforms and h_0: $A = \{F, h_0\}$.

4. The conditional probability for each transition T_j $P(T_j|A)$ is defined as $1 - PEP_j$ if hypothesis A is $A = F$, e.g. transition T_j can originate from peptidoform F, or as PEP_j otherwise. PEP_j is defined as the posterior error probability of the transition-level signal T_j as described above.

5. The marginal probability is defined as:

$$P(T) = \sum_A (\prod_j (P(T_j|A)) * P(A))$$

6. The posterior probability of peptidoform F (or h_0) for a candidate peak group is defined as:

$$P(F|T) = \frac{(\prod_j P(T_j|F)) * P(F)}{P(T)},\ P(h_0|T) = \frac{(\prod_j P(T_j|h_0)) * P(h_0)}{P(T)}$$

For each candidate peak group, the sum of all candidate peptidoform and h_0 posterior probabilities is thus 1.

F. Estimation of local and global false discovery rate

Identically as previously described, posterior error probabilities can be interpreted as local false discovery rate (fdr) and a global false discovery rate (FDR) can be derived[16,30,33]:

$$q_{PF} = \frac{\sum_{P_{PF} \in \{y | y \geq P^t_{PF}\}} PEP_{PF}}{|\{y | y \geq P^t_{PF}\}|}$$

G. Transfer of identification confidence across MS runs

Propagation of detection confidence across several MS runs has recently been developed for SWATH-MS in a method termed TRIC (TRansfer of Identification Confidence)[17]. With the same rationale as in the original publication, the model can be extended to peptidoforms. Alignment of candidate peak groups is conducted using the same chromatographic similarity, but instead of the peak group detection confidence, the peptidoform identification confidence is used.

III. BENCHMARKING USING THE SYNTHETIC PHOSPHOPEPTIDE REFERENCE DATA SET

A. Using IPF with a DIA-Umpire spectral library

Figure S3 depicts the results of the benchmark analysis of the synthetic phosphopeptide reference data set using the DIA-Umpire library. In comparison to the same analysis using the DDA-based spectral library, IPF achieves very similar performance results, i.e. receiver-operating characteristics, error-rate estimation and quantification. The main difference is the number of peptide queries.

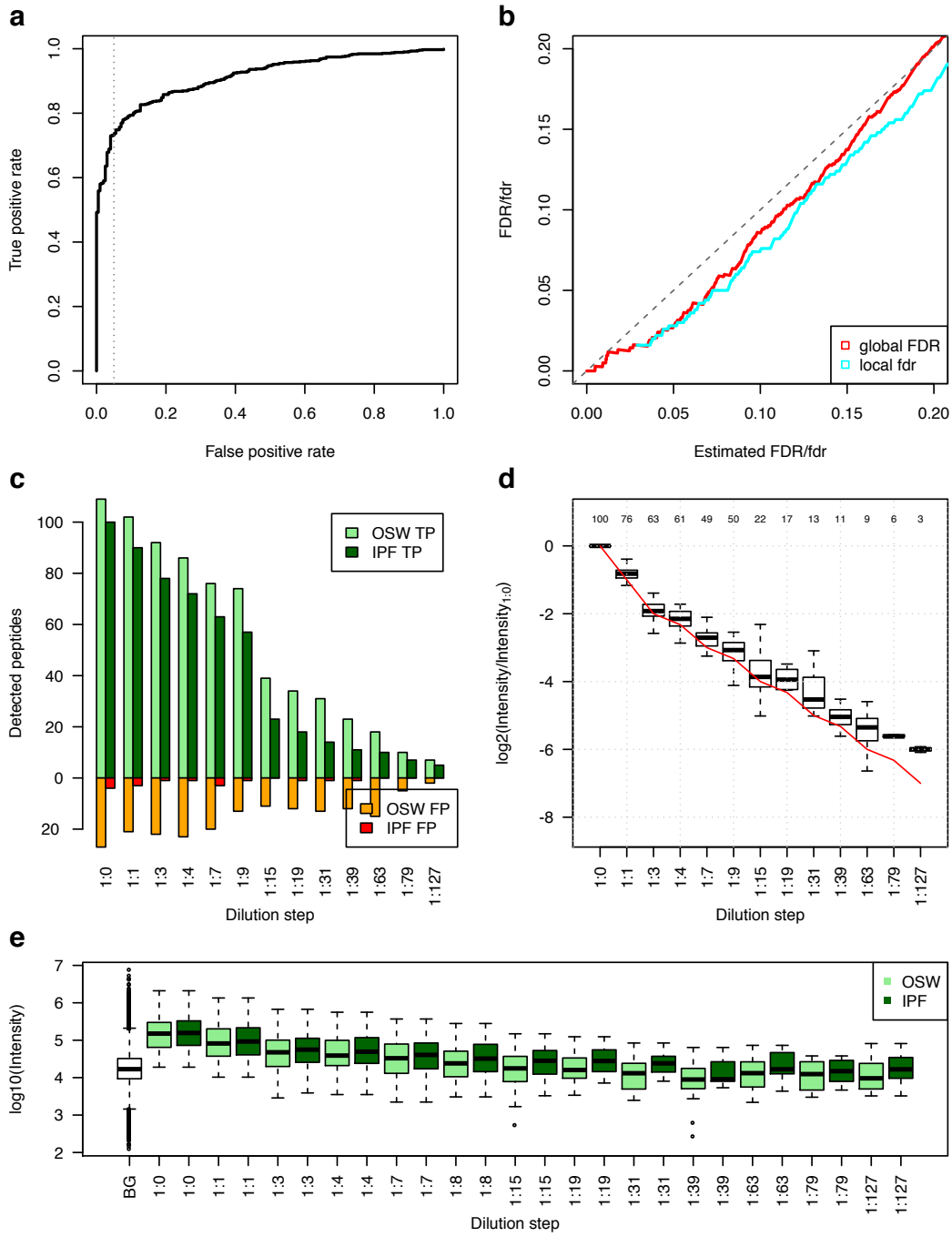

Figure S3: **Benchmarking on the synthetic phosphopeptide reference data set using the DIA-Umpire library.** Spiked-in synthetic yeast phosphopeptides[34] were measured in a 13-step dilution series with a human cell line background.

Figure S3: IPF was applied using peptide query parameters generated from a combined spectral library based on the DIA-Umpire analysis of the 13 runs. **a)** The receiver operating characteristic (ROC) indicates high sensitivity at commonly used confidence thresholds with 73.1% recovery at 5% (grey dotted line) false positive rate. **b)** The estimated global false discovery rate (FDR) or q-values are plotted against the true FDR, computed using the ground truth. The dashed diagonal line indicates the optimum. The estimated local false discovery rate (fdr) or posterior error probability (PEP) is plotted against the actual fdr, approximated using the ground truth as described previously[35] with a window size of 500. IPF enables accurate estimation in the commonly used ranges of 1-5% fdr/FDR, with a small overestimation of the error in the higher ranges. **c)** The dilution series of synthetic spiked-in standard peptides against the constant human cell line and the detected true (green) and false (red) peptidoforms at 5% FDR are depicted. The light colors (OSW) represent the detectable peptide sequence-specific peptide query-level MS2 signals. The dark colors (IPF) represent the corrected, peptidoform-specific signals. A high gain in selectivity with a small drop in sensitivity can be observed. **d)** The quantification of the peak groups (normalized against 1:0) is compared against the ground truth (red line). Until dilution step 1:15 the quantification is accurate, with a slight bias for overestimation at lower abundance dilution steps. The numbers above the boxplots indicate the number of peptides per dilution steps that are also present in the 1:0 step. **e)** The boxplots depict the intensities of correct peptidoforms and background (BG) peptides at 5% FDR. To achieve high confidence on peptidoform-level, IPF requires slightly higher signal intensities than OpenSWATH on peptide-level.

B. Comparison of false localization rates estimated by IPF and DIA-Umpire/LuciPHOr

The comparison of IPF with spectrum-centric or hybrid approaches for the identification of modified peptides, including tools like DIA-Umpire[29], MSPLIT-DIA[36] or SWATHProphetPTM[37] is not trivial, because those algorithms do not directly provide confidence metrics on the peptidoform-level. However, spectrum-centric site-localization is either supported directly or by using downstream tools[38]. We therefore compared the

site-localization component of IPF to a representative spectrum-centric site-localization workflow for DIA data.

LuciPHOr[39,40] is one of the newest and most sophisticated tools for site-localization, which can also provide confidence estimates in the form of a false localization rate (FLR). While LuciPHOr was developed for DDA spectra, it can in principle also be applied to DIA pseudo spectra. For this purpose and to make it compatible with the DIA-Umpire analysis workflow, we built a custom version of LuciPHOr 2 making use of iProphet[22] instead of PeptideProphet[21] posterior probabilities (see Methods).

For IPF, we implemented a limited model which only uses the second layer of the Bayesian hierarchical model and thus does not take into account the first layer, which is not supported by LuciPHOr 2. Confidence metrics based on these posterior probabilities can be interpreted as false localization rates, directly comparable with the spectrum-centric results reported by LuciPHOr.

To make the comparison as fair as possible, LuciPHOr used DIA-Umpire pseudo spectra and IPF used the spectral library based on the same DIA-Umpire results (without site-localization, as described above). Importantly, because not all identified spectra could be used for spectral library generation, only the intersection of peptides that both LuciPHOr and IPF could site-localize in theory was assessed. Only identified or detected peptides with an iProphet or mProphet FDR of 1% were used, respectively.

Figure S4 depicts the results of the benchmark analysis between IPF and DIA-Umpire/LuciPHOr. Both tools provide specific site-localization on the synthetic phosphopeptide reference data set and accurate estimation of the false localization rate. False positive site-localizations identified by DIA-Umpire/LuciPHOr at a high confidence threshold of 1% false positive rate (FPR) resulted in a true positive rate (TPR) of 15.5% compared to 48.5% achieved by IPF. The spike in actual FLR between $0-1\%$ estimated FLR in Figure S4b illustrates this limited specificity at the highest level of confidence. In general, IPF achieved a higher level of correct site-localizations, with a recall of 66.7% (73.5%) compared to a recall of 55.3% (59.0%) of DIA-Umpire/LuciPHOr at 5% (10%) FLR.

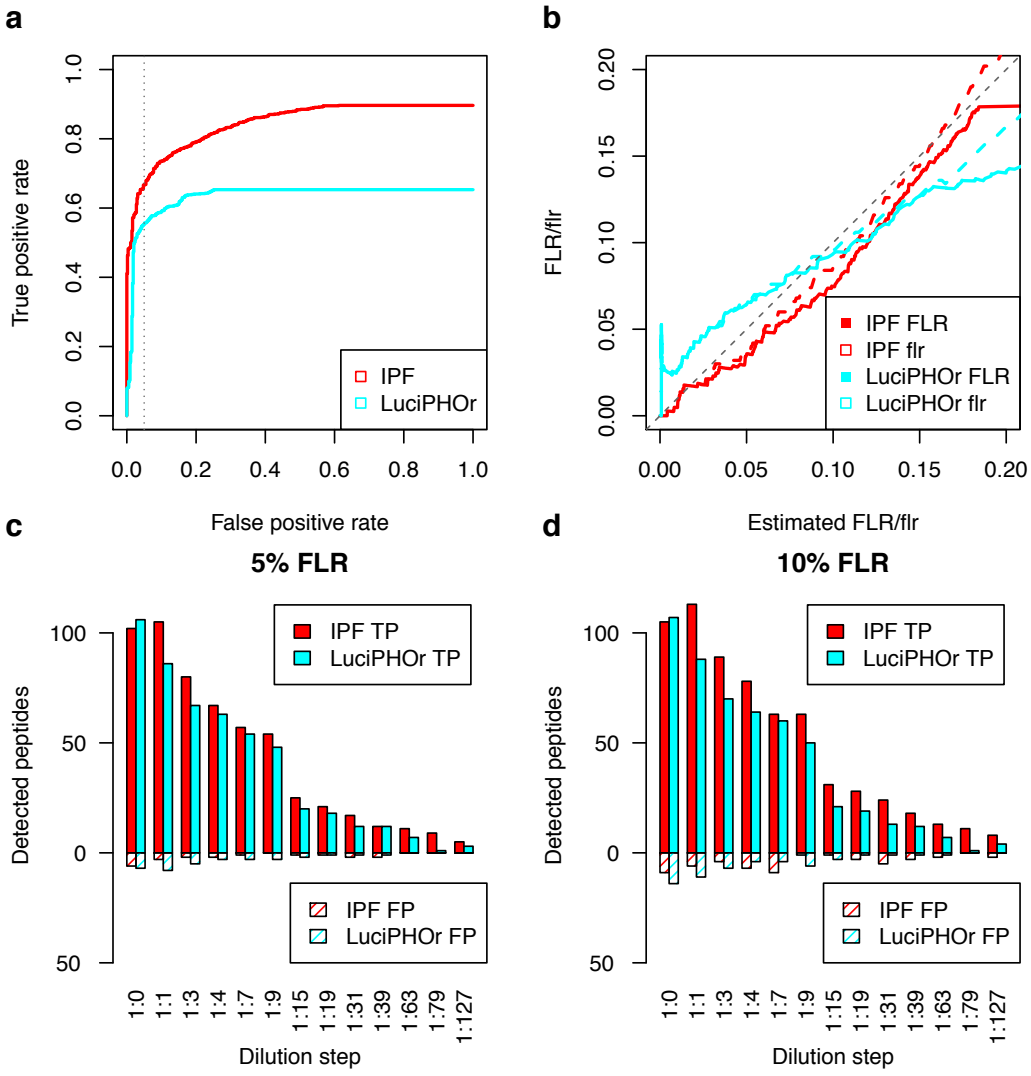

Figure S4: **Comparison of false localization rates estimated by IPF and DIA-Umpire/LuciPHOr.** The synthetic phosphopeptide reference data set analysed with DIA-Umpire was benchmarked using IPF and DIA-Umpire/LuciPHOr[39,40]. The IPF analysis was conducted using the DIA-Umpire spectral library and using a simplified Bayesian hierarchical model which estimated a false localization rate comparable to the metric reported by LuciPHOr.

Figure S4: **a)** The pseudo receiver operating characteristics (ROC) for both IPF (red) and DIA-Umpire/LuciPHOr (cyan) indicate high sensitivity and specificity at 5% (grey dotted line) false positive rate (FPR) with IPF achieving a higher true positive rate (TPR). Because neither IPF nor DIA-Umpire/LuciPHOr can identify all peptide site-localizations in all samples, they do not reach a true positive rate (TPR) of 1.0. While the TPR of LuciPHOr saturates at above 0.6, for IPF the TPR goes above 0.8, indicating higher sensitivity at the same FPR. **b)** Both IPF (red) and DIA-Umpire/LuciPHOr (cyan) accurately estimate global (FLR) and local (flr) false localization rates. However, the FLR/flr estimates of DIA-Umpire/LuciPHOr are impaired by false positive identifications at high confidence thresholds below 1% FLR/flr. **c-d)** The dilution series of synthetic spiked-in standard peptides against the constant human cell line and the detected true (solid) and false (dashed) peptide site-localizations at 5% and 10% FLR are depicted. In general, IPF (red) enables higher numbers of correct site-localizations across the dilution series than DIA-Umpire/LuciPHOr (cyan), with the effect being more pronounced at 10% FLR.

IV. COMPARISON OF IPF WITH ESTABLISHED DDA-BASED WORKFLOWS FOR IDENTIFICATION AND QUANTIFICATION OF PHOSPHOPEPTIDES

A. Scope and limitations of the comparison

Objectively comparing algorithms based on different concepts is very difficult, especially when they require different types of input data. Here we compared IPF, which conducts peptide-centric analysis of DIA data with MaxQuant[41], an established workflow conducting spectrum-centric analysis of DDA data. While we took several precautions to avoid potential bias, some inherent limitations and challenges remain in all complex comparisons:

1. Performance differences between instrument generations and types

Both MaxQuant and IPF support the analysis of data acquired on DDA- and DIA-capable QTOF and Orbitrap instruments. In our study, we analyzed data acquired on two different QTOF instrument generations, the SCIEX TripleTOF 5600 and 6600 systems. We found that the improvements of the newer 6600 series instrument translated to improved performance profiles for both DDA and DIA analysis.

Our comparison does not assess the performance of the algorithms for DDA and DIA data acquired on Orbitrap instruments. Different properties and algorithmic optimizations could potentially shift the characteristics of a DDA vs DIA comparison. However, a recently published study[42] assessed data from a latest generation Orbitrap instrument acquired in both DDA and DIA modes and suggested similar improvements for DIA over DDA acquisition, albeit for the analysis of non-modified peptides.

2. Optimal analysis strategies and parameters for MaxQuant and IPF

Both MaxQuant and IPF are part of complex workflows. MaxQuant[41] integrates Andromeda[43] for database searching and site-localization and employs the MaxLFQ[44] (match-between-run) algorithm for label-free quantification and alignment. On the other hand, IPF requires a spectral library from DDA or DIA-based spectrum-centric analyses and builds on top of OpenSWATH[1], PyProphet[4,7] and TRIC[17] for detection, quantification

and alignment. Both workflows can be optimized by tweaking parameters for specific data sets.

For MaxQuant, we used the default TOF parameters with enabled MS1 precursor-level quantification and match-between-run settings as suggested by the developers[45] (see Methods for further details and exact parameters). To our best knowledge, this resulted in an appropriate and successful analysis for both data sets, however potential optimizations that would go beyond the scope of our study could potentially further improve the performance.

To maintain the comparability between the tools, we used a MaxQuant-derived spectral library for IPF. Because we could not use our standard workflow[18] to generate consensus spectral libraries, the selection of best replicate spectra resulted in a loss of peptides and associated spectra (enriched phosphopeptide data set: 20.3%; 14-3-3 data set: 17.0%) that did not fulfill our requirements for peptide query parameters, i.e. it was not possible to derive at least six suitable transitions. We thus believe that the spectral libraries for IPF could be further optimized by applying our standard workflow to increase coverage and sensitivity. For the presented comparisons, we decided to focus on either the intersection (enriched phosphopeptide data set) or to discuss the differences in terms of covered peptides in detail (14-3-3 data set).

3. IPF and MaxQuant report results differently

The results of MaxQuant and IPF are not directly comparable, because they follow different concepts for interpretation. Andromeda filters PSMs to 1% FDR and then conducts site-localization, deriving a posterior error probability for each potential phospho-site. The results are aggregated per phospho-site and MS1-level quantification is conducted using the MaxLFQ algorithm and alignment without requiring direct spectral evidence in each run. Conversely, IPF propagates the confidence across all levels of evidence (MS2 peak group, MS1/MS2 precursors, transitions) and derives a confidence for each candidate peptide signal. Subsequent alignment by TRIC[17] is only conducted within the specified boundaries of detection confidence for each peptidoform.

We therefore conducted the comparison between IPF and MaxQuant on the level that we believe users would assess the results, namely the final quantitative matrices reported by both tools that satisfy a global confidence per peptide (see Methods for more details).

B. Benchmarking using phosphopeptide-enriched samples

To assess the scalability of IPF in comparison to established workflows for the analysis of phosphopeptide-enriched samples, we generated a data set of phosphopeptide-enriched samples of human U2OS cells. Cells were either treated with nocodazole or left untreated (control) and the resulting patterns were comparatively analyzed by IPF. Nocodazole arrests cells at the mitotic stage and thus has a substantial effect on signaling pathways involving phosphorylation[46]. We acquired ten biological replicates, processed in parallel, each for nocodazole-treated and control samples, both in DDA and DIA modes (see Methods). We then analyzed the 20 DDA runs with MaxQuant[41,43,44], which provides an integrated workflow for database search, phosphopeptide site-localization and MS1 precursor-level quantification. Based on these results, we constructed a spectral library for quantitative analysis by IPF on the corresponding 20 DIA runs. In order to provide a fair comparison between the results of MaxQuant and IPF, we restricted our comparative analysis to the intersection of phosphorylated peptides detected or identified and site-localized by both algorithms with confidence in at least one run (IPF: 1% peptidoform FDR; MaxQuant: 1% site-localization FDR), reducing the number of phosphopeptides detected by IPF to 6,260 or identified by MaxQuant to 7,136 (1,184 of which were not present in the spectral library for IPF, see Methods) with an intersection of 4,298 phosphopeptides.

We next analyzed the quantitative data matrices produced by IPF and MaxQuant across all ten replicates of each condition, considering only peak groups (IPF) or peptide precursors (MaxQuant) with at least one confident identification/detection or quantification per biological condition (Fig. S5). For the nocodazole treated and the control samples, MaxQuant achieved consistent identification and quantification among all replicates for 20.8% (22.9% after quantification) and 17.4% (16.5% after quantification, lower due to alignment with nocodazole treated runs) of all phosphopeptides. In contrast, IPF achieved both consistent detection and quantification for 62.6% (nocodazole) and 47.5% (control) of all phospho-

peptides (Fig. S5a-b). To investigate the effect that consistency of quantification has in dependency of the number of replicates, we conducted differential expression analysis using mapDIA[47] on variable numbers of sampled replicates. Depending on the number of replicates, more than 400 differentially expressed peptide precursors or peak groups were detected (Fig. S5c, significance thresholds: FDR < 0.01 & log2(FC) > 2). IPF achieved more significant results at low numbers of replicates (3 replicates: MaxQuant: 86, IPF: 134). These results demonstrate that IPF can achieve improved results on enriched phosphopeptide data sets compared to the currently employed approaches. Especially across multiple replicates, IPF achieved better consistency of detection and quantification, which lowers the number of required replicates for quantitative comparisons of different samples.

C. Quantification of phosphorylation dynamics in the 14-3-3 system

To compare the performance of IPF for the consistent quantification of phosphopeptides in a complex sample with the performance of DDA-based workflows, we analyzed the data of our previously published study of the 14-3-3 scaffold protein interactome in this context[48]. The data set consists of 6 time points measured in biological triplicates before and after stimulation by IGF1 and the samples were generated by affinity enrichment of 14-3-3 associated proteins using an affinity tagged 14-3-3 protein expressed in HEK-293 cells.

First, we conducted the DDA analysis as described above using MaxQuant (see Methods). Across the 18 runs, MaxQuant identified and quantified 535 unique phosphopeptides (site-localization FDR < 0.01), whereas IPF achieved a recovery of 314 phosphopeptides (peptidoform-level FDR < 0.01). The main difference between MaxQuant and IPF originated from 109 peptides site-localized and aligned by MaxQuant from two phospho-enriched runs, as well as 106 peptides that were not contained in the spectral library used by IPF. The enriched runs were included in the MaxQuant analysis to enable cross-run peptide identification. When comparing the consistency of quantification between the two data sets and algorithms, IPF achieved quantification across the six time points in two or more replicates for 137 phosphopeptides, whereas MaxQuant achieved the same consistency for 51 phosphopeptides (Fig. S6a). Next, we assessed the correlation of phosphopeptides, located in the 14-3-3 binding motif or outside the motif, with their associated prey proteins (Fig. S6b-c).

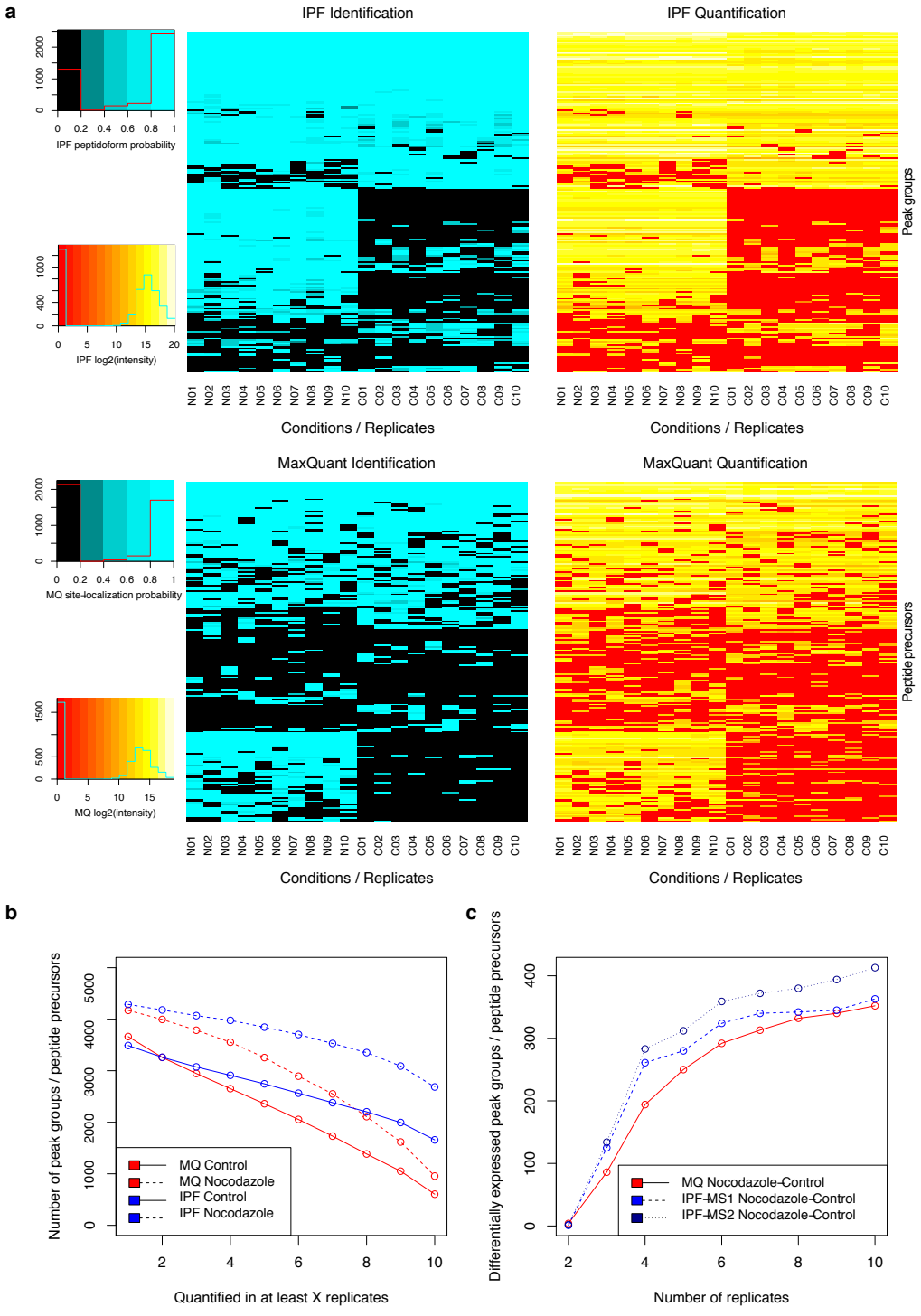

Figure S5: **Benchmarking using phosphopeptide-enriched samples.** Enriched phosphopeptide samples of a human U2OS cell line treated with nocodazole and without treatment (control) were measured in both DDA and DIA modes in each 10 replicates.

Figure S5: **a)** 200 peptides were randomly selected and the corresponding detected peak groups and peptide precursors for IPF and MaxQuant (MQ) are visualized in a heatmap (sorted by a hierarchical dendrogram for identification/detection by rows) for detectability/identification confidence (blue) and quantification (red-yellow; including alignment). IPF achieved a higher level of completeness for quantification in individual experimental conditions (Nocodazole N01-N10: 62.6%; Controls C01-C10: 47.5%) in comparison to MaxQuant (Nocodazole N01-N10: 22.9%; Controls C01-C10: 16.5%). **b)** The consistency of quantification for all intersecting peptides is depicted, where IPF provided more complete detection in replicates than MaxQuant. **c)** Differential expression analysis was conducted using mapDIA (significance thresholds: FDR < 0.01 & log2(FC) $>$ 2). For both MaxQuant and IPF on MS2 peak group (IPF-MS2) and MS1 (IPF-MS1) precursor levels, the same peptide/precursor-level model and parameters were used.

We conducted differential expression analysis and relative quantification using mapDIA as described above and assessed the distribution of the absolute Pearson correlation for consistently quantified peptides and proteins across all time points. In comparison to MaxQuant, IPF achieved a higher correlation for both motif- and other phosphopeptides, indicating more reliable profiling results. While phosphorylation in the binding motif is expected to correlate well with the protein, phosphorylation outside the motifs may also be well correlated if these sites themselves are not regulated by the stimulation. In combination, the above results suggest that the IPF analysis on the DIA data set compares favorably to established DDA-based workflows using the same amount of instrumentation time.

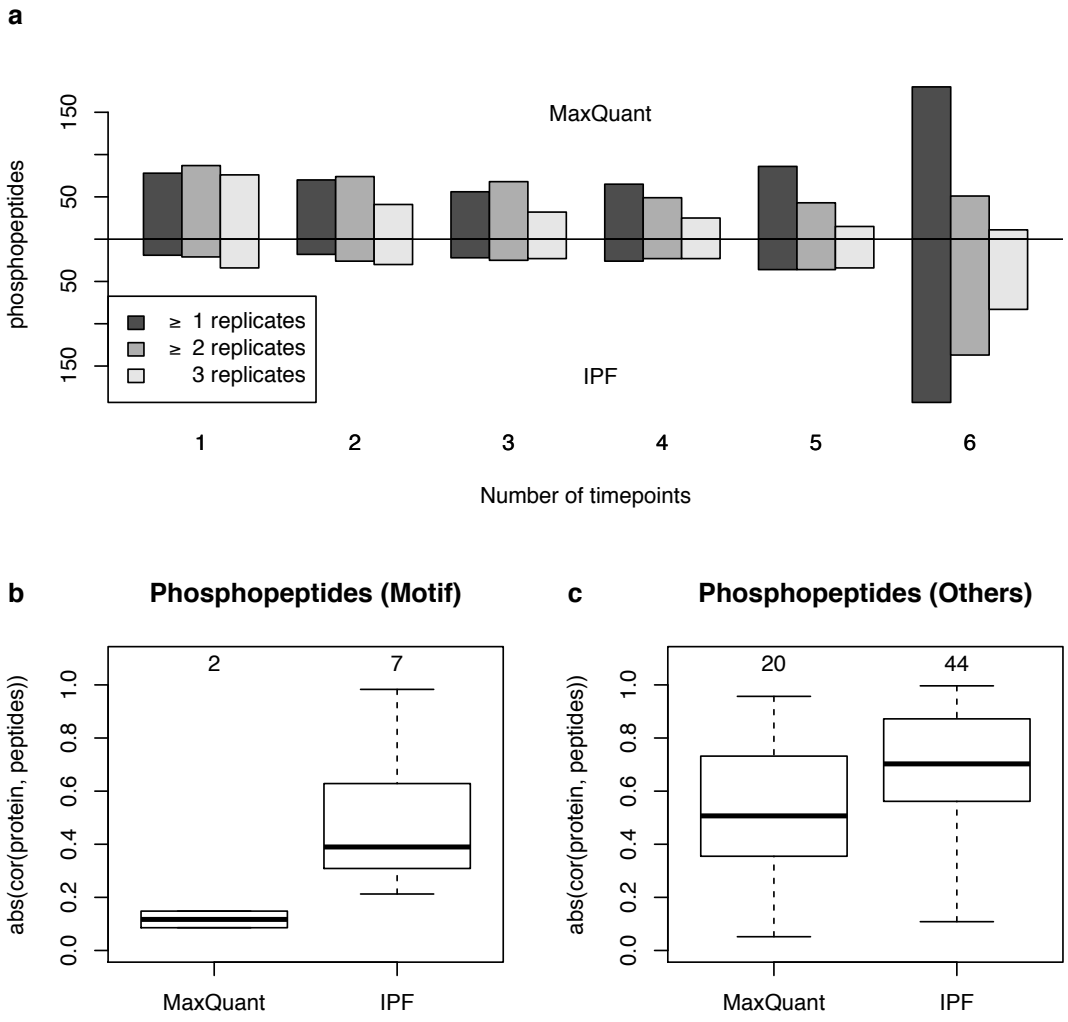

Figure S6: **Quantification of phosphorylation dynamics in the 14-3-3 system. a)** Across the full time series, IPF detected and quantified a higher number of phosphopeptides (43.6%) in two or more replicates than MaxQuant (9.5%). **b-c)** Phosphopeptides associated with the 14-3-3 binding motif are expected to correlate in abundance with their associated prey proteins. The correlation of the quantitative profiles across the full time series of consistently measured phosphopeptides (in or outside the motif) was computed and is depicted as boxplots. The number within the boxes indicate the number of data points. IPF achieves a higher absolute correlation than MaxQuant.

V. ASSESSMENT OF VARIANCE COMPONENTS OF POST-TRANSLATIONAL MODIFICATIONS IN HUMAN BLOOD PLASMA

A. Coverage of peptidoform dynamic range

Peptidoforms carrying post-translational modifications were detected and quantified over the full dynamic range across the whole twin blood plasma data set. Figure S7 depicts the distribution of modified peptidoforms for generally higher abundant proteins (top 100 proteins, selected according to summed peak group intensities) and Figure S8 visualizes the same distributions for the inverse set containing mainly lower abundant proteins.

While peptidoform abundance and coverage strongly correlates with proteoform abundance as illustrated by albumin (Figure S11), many peptidoforms carrying PTMs are detectable over the full dynamic range, also for the lower abundant proteins (Figure S8).

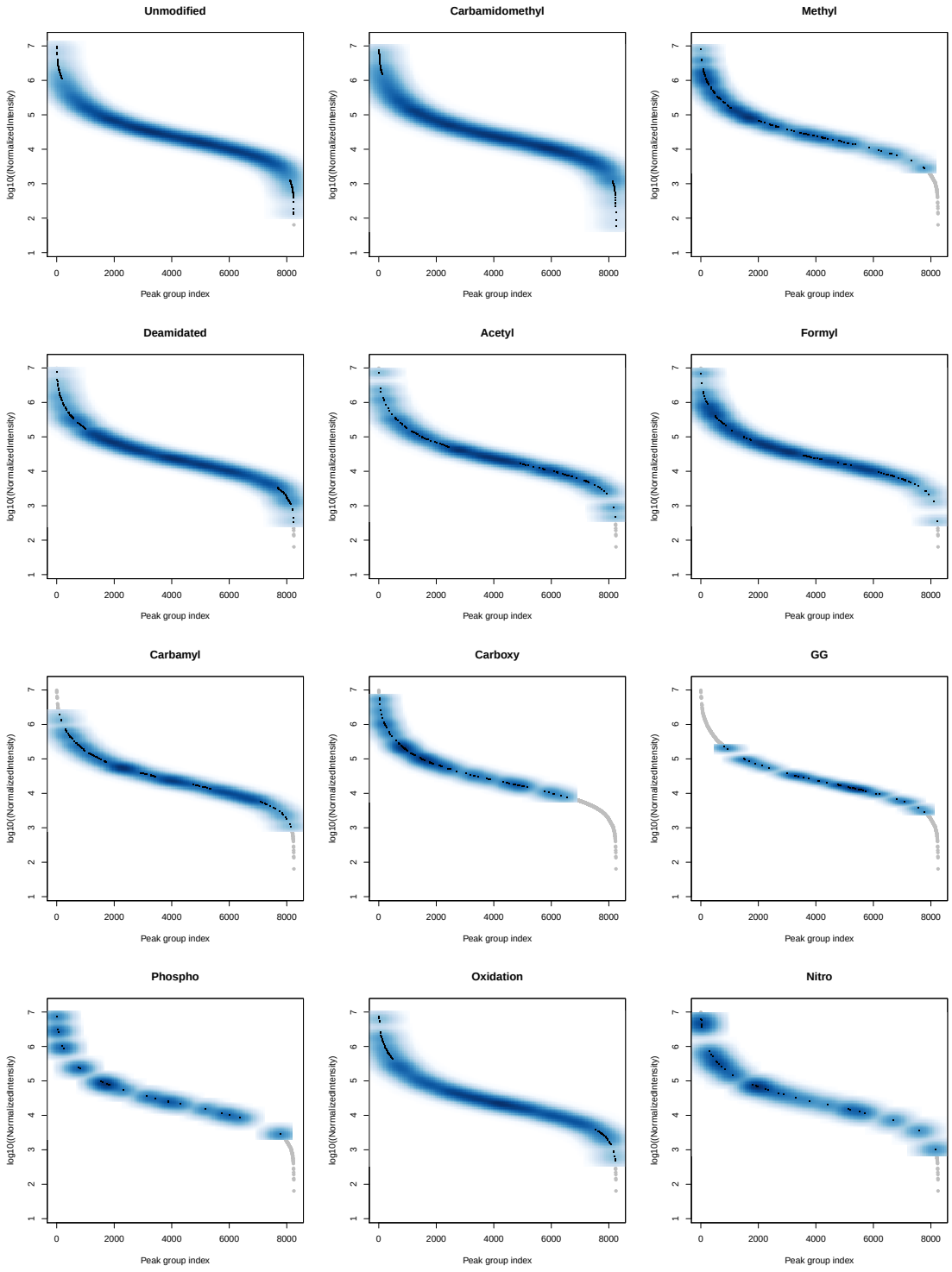

Figure S7: **Peptidoform dynamic range of top 100 most abundant proteins.** The smoothed scatter plot of peptidoform quantile normalized intensity (detected with q-value < 0.01) over all samples is depicted.

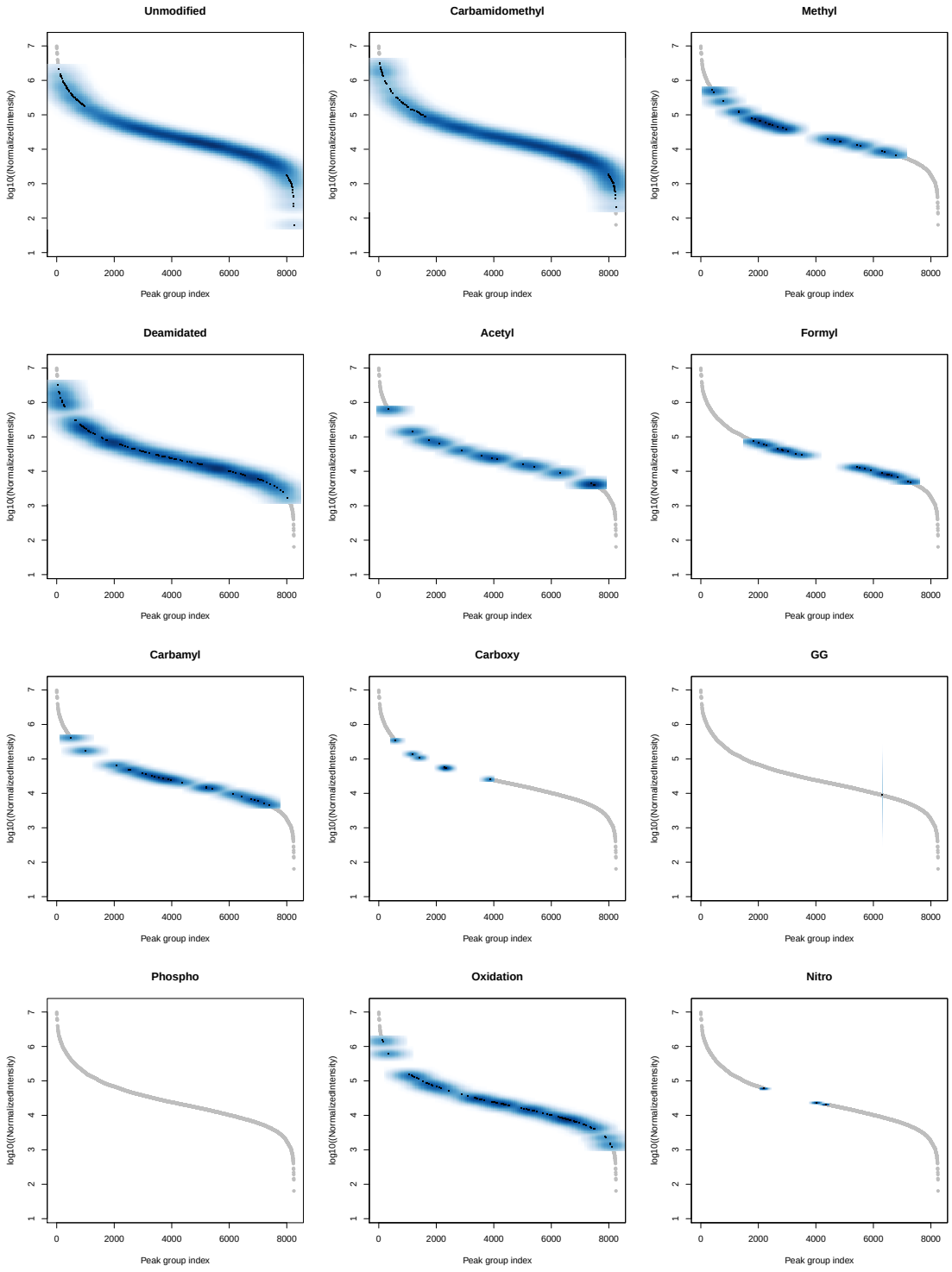

Figure S8: **Peptidoform dynamic range of lower abundant proteins.** The smoothed scatter plot of peptidoform quantile normalized intensity (detected with q-value < 0.01) over all samples is depicted.

B. Reproducibility across technical replicates

Figure S9 depicts the detectability and quantification performance across technical replicates, Figure S10 depicts the same characteristics for whole-process replicates. In general, both categories of replicates support that peptidoforms can be detected and quantified consistently.

C. Quantitative peptidoform variability of human serum albumin (ALBU)

Human serum albumin (ALBU) is the most abundant protein in the circulatory system, constituting about 55% of plasma protein mass[49]. ALBU is known to bind proteins, lipids and small molecules and it was reported that albumin and its interactors could be used as promising tool in biomarker discovery[50]. Different PTMs of ALBU (e.g. oxidation) have been reported to be involved in various of human diseases, such as cardiac ischemia[51], renal disease[52] or pulmonary hypertension[53]. We also found the variability and the dominance of ALBU in blood plasma reflected in our dataset: 440 peptidoforms (74 unmodified peptidoforms) represented by 173 backbone peptide sequences were quantified across the twin samples (see Supplementary Figure S11). They contained 426 Carbamidomethyl, 104 Formyl, 69 Carbamyl, 62 Oxidation, 31 Methyl, 21 Carboxy, 19 Deamidated, 18 GG, 16 Acetyl, 13 Nitro and 8 Phospho modifications. The variance decomposition for ALBU peptidoforms indicates for all modification types similar component levels (h2r: 4.4%, h2id: 4.2%, h2w: 15.4%, c2: 3.2%, e2: 72.8%). Compared to the original protein-level report where the unexplained effect dominated ALBU variation (e2: 87.2%), the average e2 on peptidoform-level is slightly smaller with 72.8%. Notably, the unexplained variance of ALBU peptidoforms is higher than the average level of all the other proteins, suggesting ALBU peptidoform abundances can be associated with variance not reflected by the experimental design (e.g. short-term protein concentration fluctuations, diet effects, etc.), as well as more experimental or technical variations. We found the longitudinal effect to be the most important component for ALBU variation in our data with several affected peptidoforms, indicating that ALBU abundance variability is controlled on protein-level. Declining ALBU abundance levels have been correlated with increasing age in previous studies[54]. We assessed the fold change of peptidoform quantile normalized intensity over the two time points and found

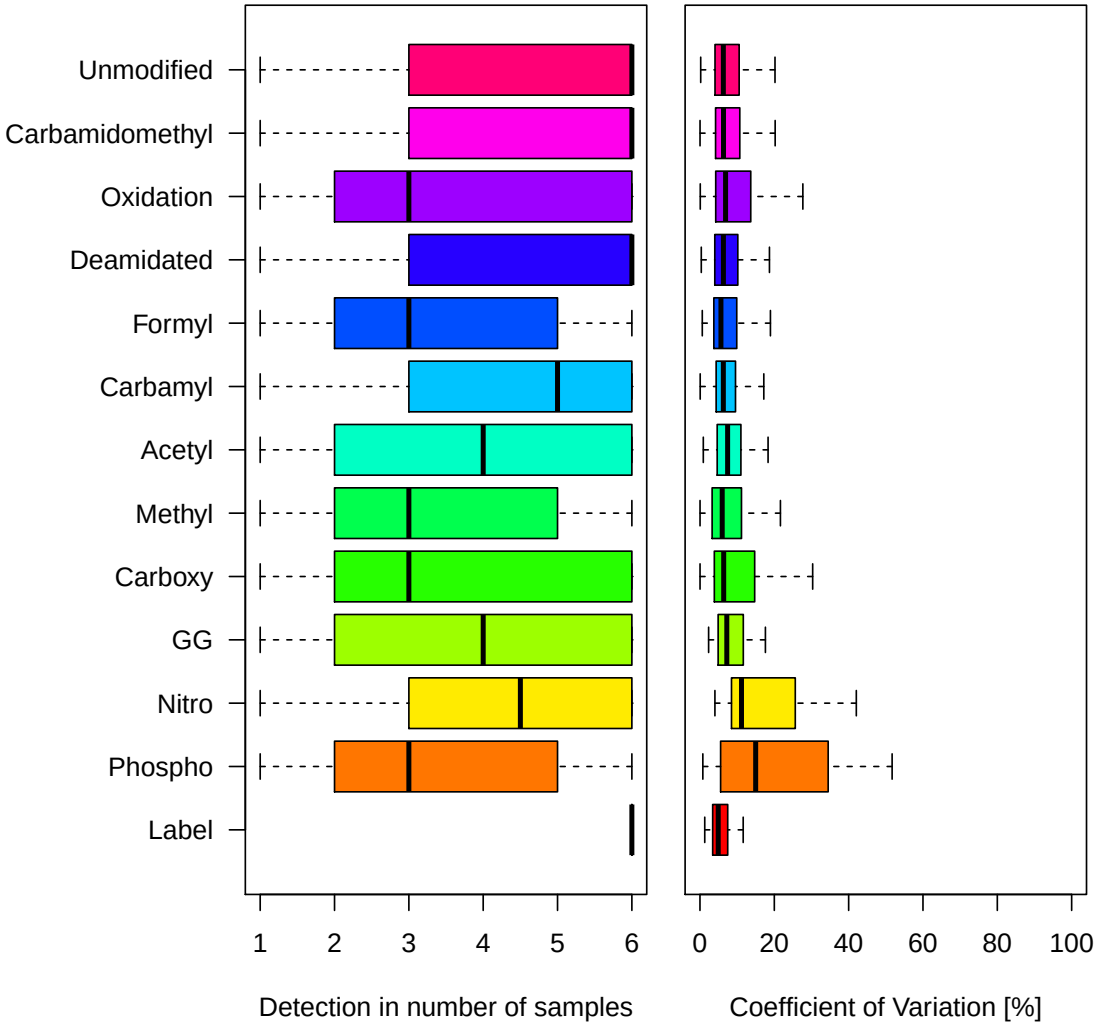

Figure S9: **Detectability and quantification of modified peptides in technical replicates of human blood plasma.** The detectability in number of technical replicates across different modification types and the coefficient of variation (CV; computed only if the peptidoform was detected in at least 2 runs) of the quantile normalized peak group intensities across different modification types is depicted. Most modified peptidoforms could consistently be detected in the majority of the technical replicates. The coefficient of variation of the intensities is commonly within the expected range (10-20%) of SWATH-MS.

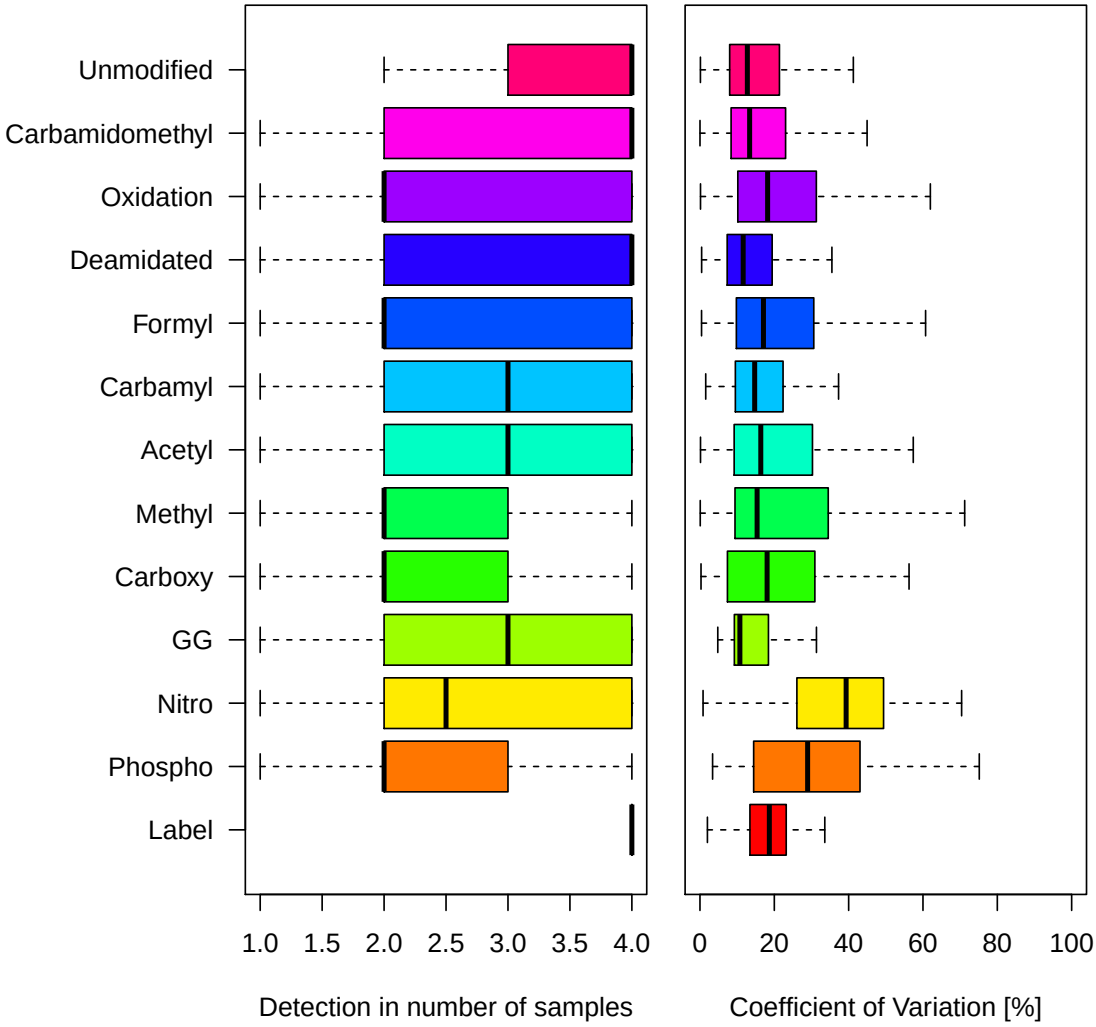

Figure S10: **Detectability and quantification of modified peptides in whole-process replicates of human blood plasma.** The detectability in number of whole-process replicates across different modification types and the coefficient of variation (CV; computed only if the peptidoform was detected in at least 2 runs) of the quantile normalized peak group intensities across different modification types is depicted. Most modified peptidoforms could consistently be detected in the majority of the whole-process replicates. The coefficient of variation of the peak group intensity is higher than for the technical replicates, representing the additional introduced variability of the sample preparation and processing steps.

only a very slight decrease in peptidoform abundance (see Supplementary Figure S12).

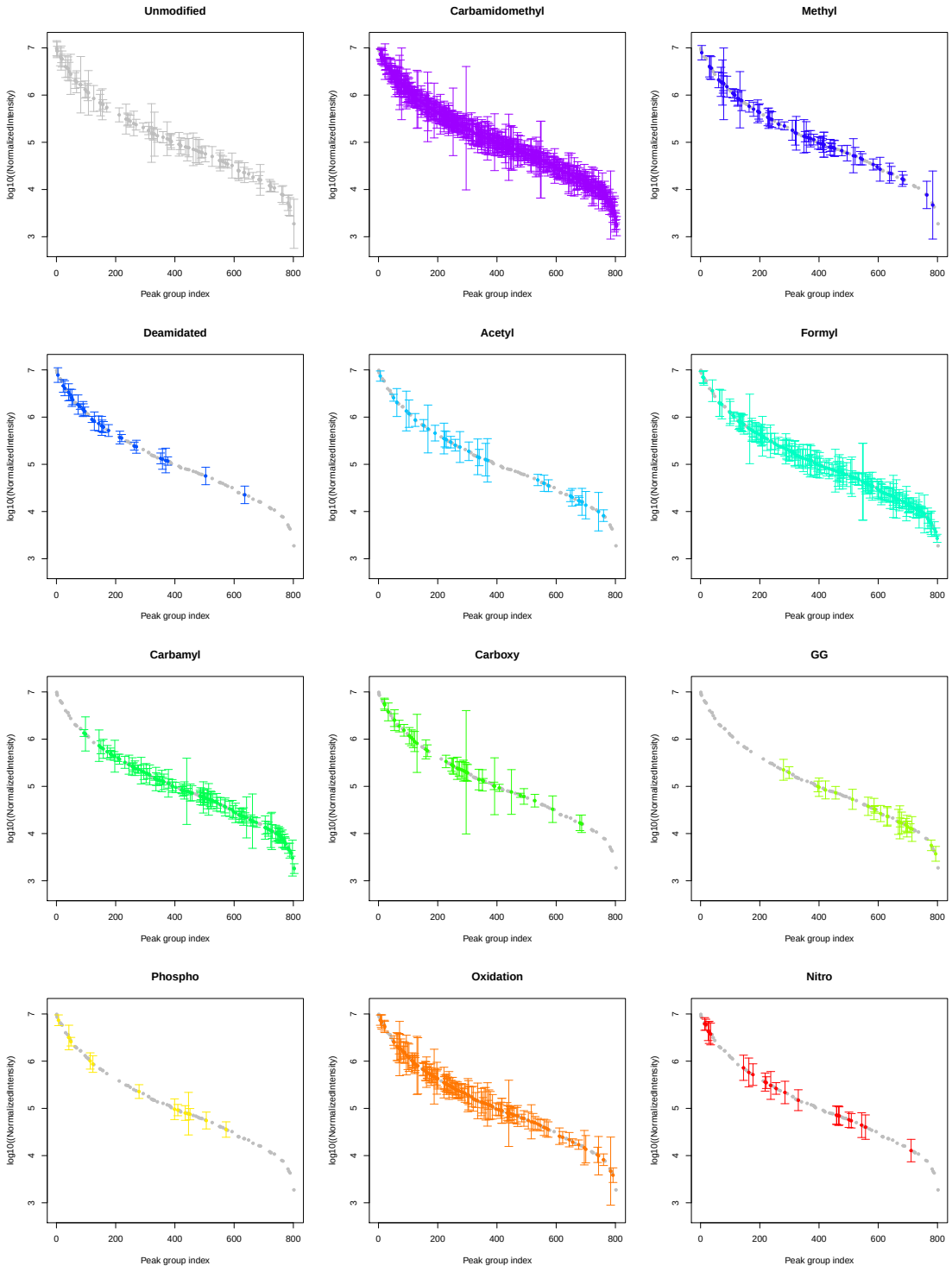

Figure S11: **ALBU modification type and peptidoform intensities distribution.** The quantitative variability (mean±sd) of peptidoform quantile normalized intensity (detected with q-value < 0.01) over all samples is depicted.

Figure S11: While the peptidoform intensity cannot be used for absolute label-free quantification, peptidoforms carrying modifications are in general distributed over the whole intensity range, which might indicate that post-translationally modified ALBU proteoforms are substantial components of the total ALBU protein mass.

D. Heritable components of ApoE isoforms E2 and E3

To demonstrate the heritable component of different peptidoforms that can be efficiently dissected using the data, we investigated ApoE, a protein associated with the high density lipoprotein (HDL) class. The three main alleles (E2, E3 & E4) of APOE only differ in one or two amino acids, and are commonly targeted for serotyping because of their involvement in e.g., Alzheimers disease (AD) risk[55]. The E4 allele is associated with increased AD risk, whereas the E2 allele is considered to protect against late-onset AD[55]. We assessed the variance components for the Cys158 peptidoforms of the E2 allele (UniProtKB: VAR_000664) and the more frequent Arg158 form of E3/E4 alleles. We found a heritable component of 56.2% (c2: 13.5% h2id: 8.1%, h2w: 3.7%, e2: 18.5%) for the E2 isoform and 17.6% (c2: 34.9% h2id: 19.2%, h2w: 1.5%, e2: 26.8%) for the E3/E4 isoform (see Supplementary Figure S13). Because for genetic analyses the sample size in this study is limited, it is very difficult to differentiate between heritable and common environment effects. For this reason, as shown previously[56], the summed heritable and common environment effects can be interpreted more robustly as family effect[57,58]. Also the e2 component can be removed to calculate the percentage of biological variability explained by different factors. Therefore, we determined 85.5% and 71.7% of the explained biological variation of APOE2 and APOE3/E4 to be associated to the family effect. It is important to notice that these components do not only indicate whether or not the peptidoforms could be detected, but also the peptidoform abundance. Taken together, our data suggests that the APOE2 allele isoform has a strong familial effect impacting both its existence and abundance in the population, suggesting that diseases related to APOE2 proteoform could have emerged with genetic or familial pattern.

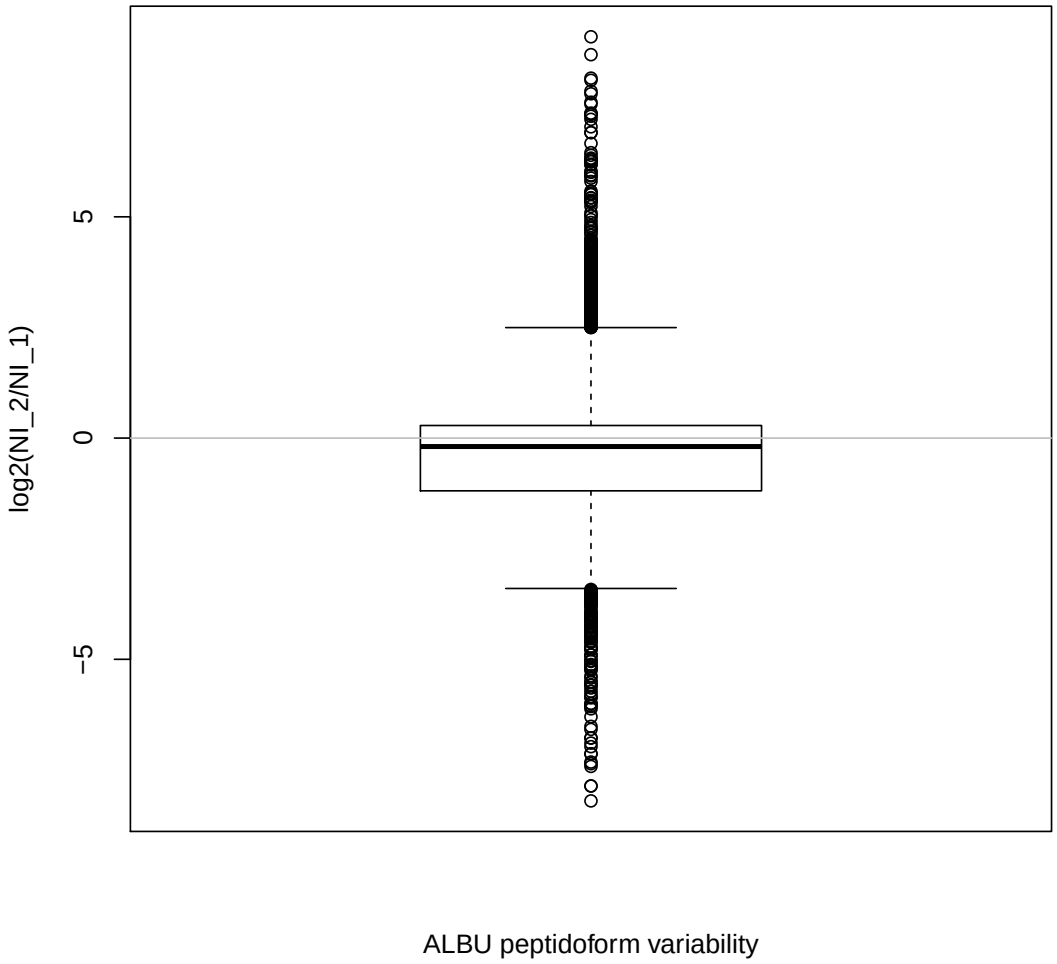

Figure S12: **Longitudinal ALBU abundance fold change.** The boxplot depicts the peptidoform abundance fold changes of all ALBU peptidoforms between time points 2 (later) and 1 (log2(NI_2/NI_1); NI: quantile normalized intensity) for all individuals. The relative ALBU peptidoform abundances remain similar over time with only a slow decrease.

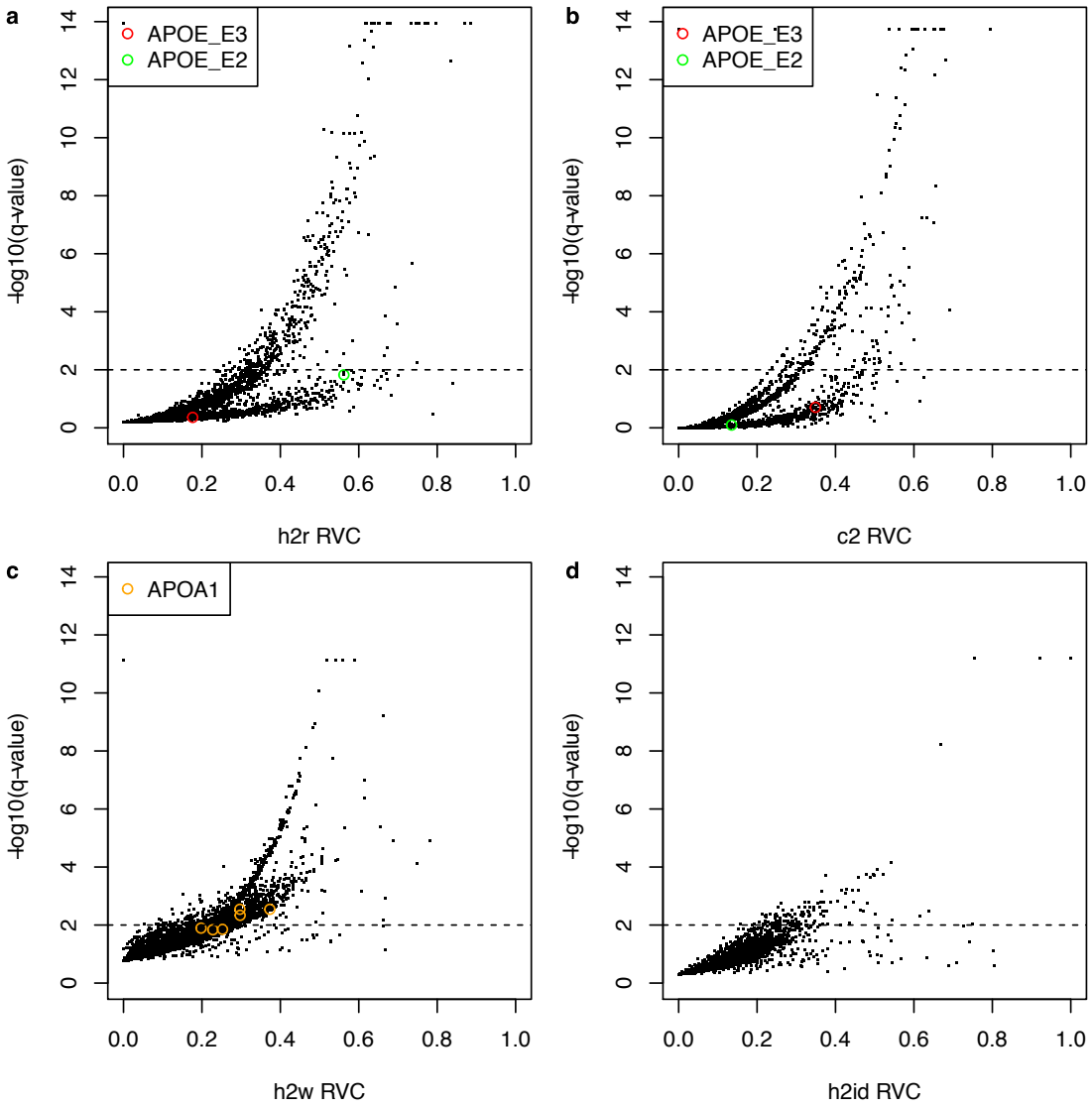

Figure S13: **Dissection of the plasma peptidoform-level variability.** The relative variance components (RVC) are plotted in a scatterplot against the -log10(q-value) per peptidoform peak group. The black dashed lines indicate significance thresholds (q-value < 0.01). The RVC of an individual peptidoform is affected by several different factors, most importantly the protein abundance and proteoform variability as well as technical effects. **a-b)** Peptides of ApoE allele variants E2 (green circles) and E3/E4 (red circles) (wild-type) were detected and quantified in the samples (Supplementary Note V.D). The heritable and common environment effects are often accounted together as "family" effects because discrimination of the two is difficult.

Figure S13: For the E2 allele, the heritable component was found to amount for 56.2% of the variance (c2: 13.5% h2id: 8.1%, h2w: 3.7%, e2: 18.5%). For the E3/E4 allele, the heritable component was found to amount for 17.6% of the variance (c2: 34.9% h2id: 19.2%, h2w: 1.5%, e2: 26.8%). **c)** The longitudinal component was found to be the major contributor to ApoA1 tryptophan oxidation (orange circles) abundance variance.

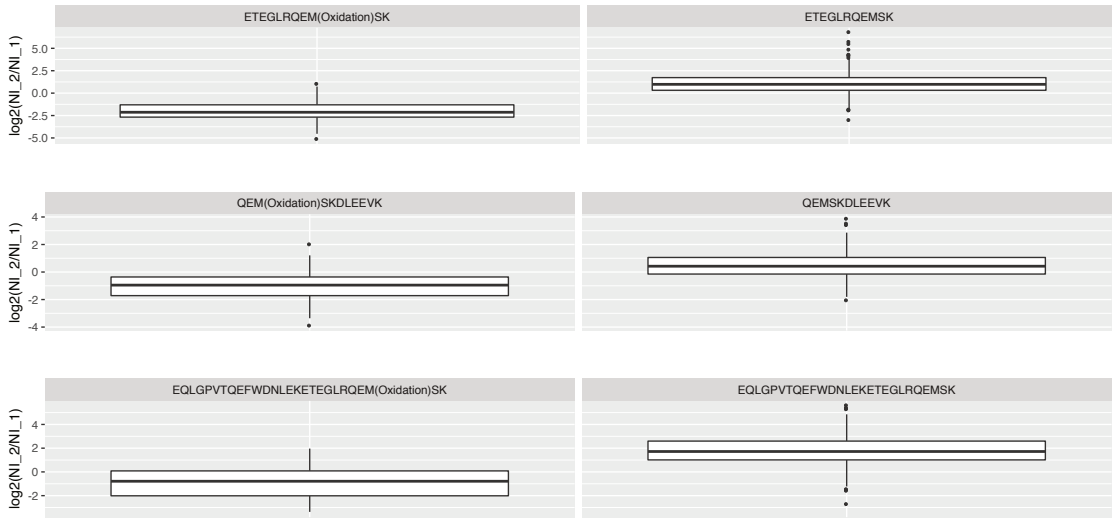

Figure S14: **oxMet86 peptidoform abundance fold changes.** The boxplots depict the peptidoform abundance fold changes between time points 2 (later) and 1 (log2(NI_2/NI_1); NI: quantile normalized intensity) for all individuals. The methionine oxidized peptidoforms (oxMet86) show a decrease, which might be induced by the longer time of sample storage and thus spontaneous methionine oxidation for the samples at the first visits.

E. Longitudinal abundance fold change of ApoA1 oxidized peptidoforms

Figure S14 depicts the oxMet86 peptidoform abundance fold change between time points 2 and 1 for each individual.

VI. IPF SOURCE CODE AND INSTRUMENT DATA

IPF is available as platform-independent open source software under the Modified BSD License and distributed as part of OpenMS[59] (`https://github.com/OpenMS`) and PyProphet[4] (`https://github.com/PyProphet`). Further documentation and instructions for usage can be found on the OpenSWATH website (`http://www.openswath.org`).

The synthetic phosphopeptide reference mass spectrometry proteomics data have been deposited to the ProteomeXchange Consortium via the PRIDE[60] partner repository `http://www.ebi.ac.uk/pride/archive/` with the dataset identifier `PXD004573`. The run filenames are listed in Table I (DDA) and Table II (DIA).

The enriched U2OS phosphopeptide mass spectrometry proteomics data have been deposited to the ProteomeXchange Consortium via the PRIDE[60] partner repository `http://www.ebi.ac.uk/pride/archive/` with the dataset identifier `PXD006056`. The run filenames are listed in Table III (DDA) and Table IV (DIA).

The 14-3-3 phosphopeptide interactomics mass spectrometry proteomics data have been deposited to the ProteomeXchange Consortium via the PRIDE[60] partner repository `http://www.ebi.ac.uk/pride/archive/` with the dataset identifier `PXD006057`.

The twin study mass spectrometry proteomics data have been deposited to the ProteomeXchange Consortium via the PRIDE[60] partner repository `http://www.ebi.ac.uk/pride/archive/` with the dataset identifier `PXD004574`.

Type	Filename
Replicate 1	chludwig_K141203_001_IDA
Replicate 2	chludwig_K141203_002_IDA
Replicate 3	chludwig_K141203_003_IDA

Table I: **Synthetic phosphopeptide reference DDA runs.**

Dilution	Filename
Dilution 1:0	chludwig_K150309_013_SW
Dilution 1:1	chludwig_K150309_012_SW
Dilution 1:3	chludwig_K150309_010_SW
Dilution 1:4	chludwig_K150309_011_SW
Dilution 1:7	chludwig_K150309_008_SW
Dilution 1:9	chludwig_K150309_009_SW
Dilution 1:15	chludwig_K150309_006b_SW
Dilution 1:19	chludwig_K150309_007b_SW
Dilution 1:31	chludwig_K150309_004b_SW
Dilution 1:39	chludwig_K150309_005b_SW
Dilution 1:63	chludwig_K150309_002b_SW
Dilution 1:79	chludwig_K150309_003b_SW
Dilution 1:127	chludwig_K150309_001b_SW

Table II: **Synthetic phosphopeptide reference DIA runs.**

Treatment	Replicate	Filename
Control	1	yanliu_I170114_001_PhosCyc1_shotgun
Control	2	yanliu_I170114_005_PhosCyc2_shotgun
Control	3	yanliu_I170114_009_PhosCyc3_shotgun
Control	4	yanliu_I170114_013_PhosCyc4_shotgun
Control	5	yanliu_I170114_017_PhosCyc5_shotgun
Control	6	yanliu_I170114_021_PhosCyc6_shotgun
Control	7	yanliu_I170114_025_PhosCyc7_shotgun
Control	8	yanliu_I170114_029_PhosCyc8_shotgun
Control	9	yanliu_I170114_033_PhosCyc9_shotgun
Control	10	yanliu_I170114_037_PhosCyc10_shotgun
Nocodazole	1	yanliu_I170114_002_PhosNoco1_shotgun
Nocodazole	2	yanliu_I170114_007_PhosNoco2_shotgun
Nocodazole	3	yanliu_I170114_011_PhosNoco3_shotgun
Nocodazole	4	yanliu_I170114_015_PhosNoco4_shotgun
Nocodazole	5	yanliu_I170114_019_PhosNoco5_shotgun
Nocodazole	6	yanliu_I170114_023_PhosNoco6_shotgun
Nocodazole	7	yanliu_I170114_027_PhosNoco7_shotgun
Nocodazole	8	yanliu_I170114_031_PhosNoco8_shotgun
Nocodazole	9	yanliu_I170114_035_PhosNoco9_shotgun
Nocodazole	10	yanliu_I170114_039_PhosNoco10_shotgun

Table III: **Enriched U2OS phosphopeptide DDA runs.**

Treatment	Replicate	Filename
Control	1	yanliu_I170114_003_PhosCyc1_SW
Control	2	yanliu_I170114_006_PhosCyc2_SW
Control	3	yanliu_I170114_010_PhosCyc3_SW
Control	4	yanliu_I170114_014_PhosCyc4_SW
Control	5	yanliu_I170114_018_PhosCyc5_SW
Control	6	yanliu_I170114_022_PhosCyc6_SW
Control	7	yanliu_I170114_026_PhosCyc7_SW
Control	8	yanliu_I170114_041_PhosCyc8_SW_rep
Control	9	yanliu_I170114_034_PhosCyc9_SW
Control	10	yanliu_I170114_038_PhosCyc10_SW
Nocodazole	1	yanliu_I170114_004_PhosNoco1_SW
Nocodazole	2	yanliu_I170114_008_PhosNoco2_SW
Nocodazole	3	yanliu_I170114_012_PhosNoco3_SW
Nocodazole	4	yanliu_I170114_016_PhosNoco4_SW
Nocodazole	5	yanliu_I170114_020_PhosNoco5_SW
Nocodazole	6	yanliu_I170114_024_PhosNoco6_SW
Nocodazole	7	yanliu_I170114_028_PhosNoco7_SW
Nocodazole	8	yanliu_I170114_032_PhosNoco8_SW
Nocodazole	9	yanliu_I170114_036_PhosNoco9_SW
Nocodazole	10	yanliu_I170114_040_PhosNoco10_SW

Table IV: **Enriched U2OS phosphopeptide DIA runs.**

VII. REFERENCES

[1] Röst, H. L. *et al.* OpenSWATH enables automated, targeted analysis of data-independent acquisition MS data. *Nat. Biotechnol.* **32**, 219–223 (2014).

[2] Kohlbacher, O. *et al.* TOPP–the OpenMS proteomics pipeline. *Bioinformatics* **23**, e191–e197 (2007).

[3] Sturm, M. *et al.* OpenMS – An open-source software framework for mass spectrometry. *BMC Bioinformatics* **9**, 163 (2008).

[4] Teleman, J. *et al.* DIANA-algorithmic improvements for analysis of data-independent acquisition MS data. *Bioinformatics* **31**, 555–562 (2014).

[5] Lawrence, R. T., Searle, B. C., Llovet, A. & Villén, J. Plug-and-play analysis of the human phosphoproteome by targeted high-resolution mass spectrometry. *Nat. Methods* **13**, 431–434 (2016).

[6] Deutsch, E. W. *et al.* TraML–A Standard Format for Exchange of Selected Reaction Monitoring Transition Lists. *Mol. Cell. Proteomics* **11**, R111.015040–R111.015040 (2012).

[7] Reiter, L. *et al.* mProphet: automated data processing and statistical validation for large-scale SRM experiments. *Nat. Methods* **8**, 430–435 (2011).

[8] Gillet, L. C. *et al.* Targeted data extraction of the MS/MS spectra generated by data-independent acquisition: a new concept for consistent and accurate proteome analysis. *Mol. Cell. Proteomics* **11**, O111.016717–O111.016717 (2012).

[9] Röst, H., Malmström, L. & Aebersold, R. A computational tool to detect and avoid redundancy in selected reaction monitoring. *Mol. Cell. Proteomics* **11**, 540–549 (2012).

[10] Sherman, J., Molloy, M. P. & Burlingame, A. L. Why complexity and entropy matter: Information, posttranslational modifications, and assay fidelity. *Proteomics* **12**, 1147–1150 (2012).

[11] Rardin, M. J. *et al.* MS1 Peptide Ion Intensity Chromatograms in MS2 (SWATH) Data Independent Acquisitions. Improving Post Acquisition Analysis of Proteomic Experiments. *Mol. Cell. Proteomics* **14**, 2405–2419 (2015).

[12] Käll, L., Canterbury, J. D., Weston, J., Noble, W. S. & MacCoss, M. J. Semi-supervised learning for peptide identification from shotgun proteomics datasets. *Nat. Methods* **4**, 923–925 (2007).

[13] Käll, L., Storey, J. D. & Noble, W. S. Non-parametric estimation of posterior error proba-

bilities associated with peptides identified by tandem mass spectrometry. *Bioinformatics* **24**, i42–8 (2008).

[14] Käll, L., Storey, J. D. & Noble, W. S. QVALITY: non-parametric estimation of q-values and posterior error probabilities. *Bioinformatics* **25**, 964–966 (2009).

[15] Sherman, J., McKay, M. J., Ashman, K. & Molloy, M. P. Unique ion signature mass spectrometry, a deterministic method to assign peptide identity. *Mol. Cell. Proteomics* **8**, 2051–2062 (2009).

[16] Käll, L., Storey, J. D., MacCoss, M. J. & Noble, W. S. Posterior Error Probabilities and False Discovery Rates: Two Sides of the Same Coin. *J. Proteome Res.* **7**, 40–44 (2007).

[17] Röst, H. L. *et al.* TRIC: an automated alignment strategy for reproducible protein quantification in targeted proteomics. *Nat. Methods* **13**, 777–783 (2016).

[18] Schubert, O. T. *et al.* Building high-quality assay libraries for targeted analysis of SWATH MS data. *Nat. Protoc.* **10**, 426–441 (2015).

[19] Eng, J. K., McCormack, A. L. & Yates, J. R. An approach to correlate tandem mass spectral data of peptides with amino acid sequences in a protein database. *J. Am. Soc. Mass Spectrom.* **5**, 976–989 (1994).

[20] Eng, J. K., Jahan, T. A. & Hoopmann, M. R. Comet: An open-source MS/MS sequence database search tool. *Proteomics* **13**, 22–24 (2013).

[21] Keller, A., Nesvizhskii, A. I., Kolker, E. & Aebersold, R. Empirical statistical model to estimate the accuracy of peptide identifications made by MS/MS and database search. *Anal. Chem.* **74**, 5383–5392 (2002).

[22] Shteynberg, D. *et al.* iProphet: multi-level integrative analysis of shotgun proteomic data improves peptide and protein identification rates and error estimates. *Mol. Cell. Proteomics* **10**, M111.007690 (2011).

[23] Lam, H. *et al.* Building consensus spectral libraries for peptide identification in proteomics. *Nat. Methods* **5**, 873–875 (2008).

[24] Escher, C. *et al.* Using iRT, a normalized retention time for more targeted measurement of peptides. *Proteomics* **12**, 1111–1121 (2012).

[25] Toprak, U. H. *et al.* Conserved Peptide fragmentation as a benchmarking tool for mass spectrometers and a discriminating feature for targeted proteomics. *Mol. Cell. Proteomics* **13**, 2056–2071 (2014).

[26] Elias, J. E. & Gygi, S. P. Target-decoy search strategy for increased confidence in large-scale protein identifications by mass spectrometry. *Nat. Methods* **4**, 207–214 (2007).

[27] Schilling, B. *et al.* Platform-independent and label-free quantitation of proteomic data using MS1 extracted ion chromatograms in skyline: application to protein acetylation and phosphorylation. *Mol. Cell. Proteomics* **11**, 202–214 (2012).

[28] Walzthoeni, T. *et al.* xTract: software for characterizing conformational changes of protein complexes by quantitative cross-linking mass spectrometry. *Nat. Methods* **12**, 1185–1190 (2015).

[29] Tsou, C.-C. *et al.* DIA-Umpire: comprehensive computational framework for data-independent acquisition proteomics. *Nat. Methods* **12**, 258–264 (2015).

[30] Nesvizhskii, A. I., Keller, A., Kolker, E. & Aebersold, R. A statistical model for identifying proteins by tandem mass spectrometry. *Anal. Chem.* **75**, 4646–4658 (2003).

[31] Serang, O. & Noble, W. A review of statistical methods for protein identification using tandem mass spectrometry. *Stat Interface* **5**, 3–20 (2012).

[32] Serang, O., MacCoss, M. J. & Noble, W. S. Efficient Marginalization to Compute Protein Posterior Probabilities from Shotgun Mass Spectrometry Data. *J. Proteome Res.* **9**, 5346–5357 (2010).

[33] Efron, B., Tibshirani, R., Storey, J. D. & Tusher, V. Empirical Bayes Analysis of a Microarray Experiment. *JASA* **96**, 1151–1160 (2001).

[34] Soste, M. *et al.* A sentinel protein assay for simultaneously quantifying cellular processes. *Nat. Methods* **11**, 1045–1048 (2014).

[35] Choi, H., Ghosh, D. & Nesvizhskii, A. I. Statistical Validation of Peptide Identifications in Large-Scale Proteomics Using the Target-Decoy Database Search Strategy and Flexible Mixture Modeling. *J. Proteome Res.* **7**, 286–292 (2007).

[36] Wang, J. *et al.* MSPLIT-DIA: sensitive peptide identification for data-independent acquisition. *Nat. Methods* **12**, 1106–1108 (2015).

[37] Keller, A. *et al.* Opening a SWATH Window on Posttranslational Modifications: Automated Pursuit of Modified Peptides. *Mol. Cell. Proteomics* **15**, 1151–1163 (2016).

[38] Chalkley, R. J. & Clauser, K. R. Modification Site Localization Scoring: Strategies and Performance. *Mol. Cell. Proteomics* **11**, 3–14 (2012).

[39] LuciPHOr: Algorithm for Phosphorylation Site Localization with False Localization Rate

Estimation Using Modified Target-Decoy Approach. *Mol. Cell. Proteomics* **12**, 3409–3419 (2013).

[40] Fermin, D., Avtonomov, D., Choi, H. & Nesvizhskii, A. LuciPHOr2: site localization of generic post-translational modifications from tandem mass spectrometry data. *Bioinformatics* (2014).

[41] Cox, J. & Mann, M. MaxQuant enables high peptide identification rates, individualized p.p.b.-range mass accuracies and proteome-wide protein quantification. *Nat. Biotechnol.* **26**, 1367–1372 (2008).

[42] Bruderer, R. *et al.* Heralds of parallel MS: Data-independent acquisition surpassing sequential identification of data dependent acquisition in proteomics. *Mol. Cell. Proteomics* mcp.M116.065730 (2017).

[43] Cox, J. *et al.* Andromeda: a peptide search engine integrated into the MaxQuant environment. *J. Proteome Res.* **10**, 1794–1805 (2011).

[44] Cox, J. *et al.* Accurate proteome-wide label-free quantification by delayed normalization and maximal peptide ratio extraction, termed MaxLFQ. *Mol. Cell. Proteomics* **13**, 2513–2526 (2014).

[45] Tyanova, S. *et al.* The Perseus computational platform for comprehensive analysis of (prote)omics data. *Nat. Methods* (2016).

[46] Nagano, K. *et al.* Phosphoproteomic analysis of distinct tumor cell lines in response to nocodazole treatment. *Proteomics* **9**, 2861–2874 (2009).

[47] Teo, G. *et al.* mapDIA: Preprocessing and statistical analysis of quantitative proteomics data from data independent acquisition mass spectrometry. *J. Proteomics* **129**, 108–120 (2015).

[48] Collins, B. C. *et al.* Quantifying protein interaction dynamics by SWATH mass spectrometry: application to the 14-3-3 system. *Nat. Methods* **10**, 1246–1253 (2013).

[49] Anderson, N. L. & Anderson, N. G. The human plasma proteome: history, character, and diagnostic prospects. *Mol. Cell. Proteomics* **1**, 845–867 (2002).

[50] Gundry, R. L., Fu, Q., Jelinek, C. A., van Eyk, J. E. & Cotter, R. J. Investigation of an albumin-enriched fraction of human serum and its albuminome. *Proteomics Clin. Appl.* **1**, 73–88 (2007).

[51] Jelinek, C. A. *Characterizing the post-translational modifications of human serum albumin as they correlate to cardiac ischemia* (John Hopkins University, 2012).

[52] Donadio, C., Tognotti, D. & Donadio, E. Albumin modification and fragmentation in renal

disease. *Clin. Chim. Acta* **413**, 391–395 (2012).

[53] Odhiambo, A. *et al.* Identification of oxidative post-translational modification of serum albumin in patients with idiopathic pulmonary arterial hypertension and pulmonary hypertension of sickle cell anemia. *Rapid Commun. Mass Spectrom.* **21**, 2195–2203 (2007).

[54] Miyake, M., Ogawa, Y. & Yoshida, Y. Seven-year large cohort study for the association of serum albumin level and aging among community dwelling elderly. *Int J Anal Bio-Sci* **4**, 281–286 (2011).

[55] Nishimura, M., Satoh, M., Matsushita, K. & Nomura, F. How proteomic ApoE serotyping could impact Alzheimer's disease risk assessment: genetic testing by proteomics. *Expert Rev. Proteomics* **11**, 405–407 (2014).

[56] Liu, Y. *et al.* Quantitative variability of 342 plasma proteins in a human twin population. *Mol. Syst. Biol.* **11**, 786–786 (2015).

[57] Kato, B. S. *et al.* Variance decomposition of protein profiles from antibody arrays using a longitudinal twin model. *Proteome Sci.* **9**, 73 (2011).

[58] Nicholson, G. *et al.* Human metabolic profiles are stably controlled by genetic and environmental variation. *Mol. Syst. Biol.* **7**, 525–525 (2011).

[59] Röst, H. L. *et al.* OpenMS: a flexible open-source software platform for mass spectrometry data analysis. *Nat. Methods* **13**, 741–748 (2016).

[60] Vizcaíno, J. A. *et al.* 2016 update of the PRIDE database and its related tools. *Nucleic Acids Res.* **44**, D447–56 (2016).